ERDC/CRREL TR-22-12

US Army Corps of Engineers®
Engineer Research and Development Center

ERDC ENGINEER RESEARCH & DEVELOPMENT CENTER

Environmental Security Technology Certification Program (ESTCP)

Determination of Residual Low-Order Detonation Particle Characteristics from Composition B Mortar Rounds

Matthew F. Bigl, Samuel A. Beal, and Charles A. Ramsey

August 2022

Cold Regions Research and Engineering Laboratory

The US Army Engineer Research and Development Center (ERDC) solves the nation's toughest engineering and environmental challenges. ERDC develops innovative solutions in civil and military engineering, geospatial sciences, water resources, and environmental sciences for the Army, the Department of Defense, civilian agencies, and our nation's public good. Find out more at www.erdc.usace.army.mil.

To search for other technical reports published by ERDC, visit the ERDC online library at https://erdclibrary.on.worldcat.org/discovery.

Environmental Security Technology
Certification Program (ESTCP)

ERDC/CRREL TR-22-12
August 2022

Determination of Residual Low-Order Detonation Particle Characteristics from Composition B Mortar Rounds

Matthew F. Bigl and Samuel A. Beal

US Army Engineer Research and Development Center (ERDC)
Cold Regions Research and Engineering Laboratory (CRREL)
72 Lyme Road
Hanover, NH 03755-1290

Charles A. Ramsey

EnviroStat, Inc.
PO Box 339
Vail, AZ 85641

Final Technical Report (TR)

Prepared for Strategic Environmental Research and Development Program
Environmental Security Technology Certification Program
Environmental Restoration Program Area
4800 Mark Center Drive, Suite 16F16
Alexandria, VA 22350-3605

Under Environmental Restoration Program project number ER18-5105, "Determination of Residual Low-Order Detonation Particle Characteristics," through MIPRs W74RDV80715663, W74RDV80715688, W74RDV90156248, and W74RDV90497295

Abstract

Empirical measurements of the spatial distribution, particle-size distribution, mass, morphology, and energetic composition of particles from low-order (LO) detonations are critical to accurately characterizing environmental impacts on military training ranges. This study demonstrated a method of generating and characterizing LO-detonation particles, previously applied to insensitive munitions, to 81 mm mortar rounds containing the conventional explosive formulation Composition B. The three sampled rounds had estimated detonation efficiencies ranging from 64% to 82% as measured by sampled residual energetic material. For all sampled rounds, energetic deposition rates were highest closer to the point of detonation; however, the mass per radial meter varied. The majority of particles (>60%), by mass, were <2 mm in size. However, the spatial distribution of the <2 mm particles from the point of detonation varied between the three sampled rounds. In addition to the particle-size-distribution results, several method performance observations were made, including command-detonation configurations, sampling quality control, particle-shape influence on laser-diffraction particle-size analysis (LD-PSA), and energetic purity trends. Overall, this study demonstrated the successful characterization of Composition B LO-detonation particles from command detonation through combined analysis by LD-PSA and sieving.

Contents

Figures and Tables

Figures

Tables

Preface

This research was conducted for the Strategic Environmental Research and Development Program (SERDP) Environmental Security and Technology Certification Program (ESTCP) under Environmental Restoration Program project number ER18-5105, "Determination of Residual Low-Order Detonation Particle Characteristics." Funding was provided by MIPRs W74RDV80715663, W74RDV80715688, W74RDV90156248, and W74RDV90497295. Dr. Herb Nelson was executive director for SERDP-ESTCP, and Dr. Andrea Leeson was deputy director and project monitor.

This report was prepared by the Engineering Resources Branch (ERB) and the Biogeochemical Sciences Branch (BSB) of the Research and Engineering Division, US Army Engineer Research and Development Center, Cold Regions Research and Engineering Laboratory (ERDC-CRREL). Researchers from ERDC-CRREL collaborated with EnviroStat, Inc, of Vail, Arizona. At the time of publication, Dr. Melisa Nallar was acting chief, ERB; Mr. Nathan Lamie was chief, BSB; and Caitlin A. Callaghan was division chief. The acting deputy director of ERDC-CRREL was Mr. Bryan E. Baker, and the director was Dr. Joseph L. Corriveau.

The authors acknowledge Mr. Michael R. Walsh, Dr. Susan Taylor, Ms. Katrina Burch, Mr. Brandon Booker, and Ms. Lauren Farnsworth of ERDC-CRREL for experimentation support and Mr. Arthur Gelvin, Ms. Stephanie Saari, Ms. Ashley Mossell, and Ms. Patricia Nelson of ERDC-CRREL for field support. The authors would also like to thank the 716th Explosive Ordnance Disposal Company and the Range Control Office of Fort Richardson for coordination and field support. Manuscript review was coordinated with Joint Program Executive Office Armaments and Ammunition. Dr. Jay Clausen and Dr. Warren Kadoya, ERDC-CRREL, provided manuscript technical review comments.

Portions of this report have been modified and reprinted from M. F. Bigl, S. A. Beal, and C. A. Ramsey, *Determination of Residual Low-Order Detonation Particle Characteristics from IMX-104 Mortar Rounds*, ERDC/CRREL TR-21-12 (Hanover, NH: U.S. Army Engineer Research and Development Center, Cold Regions Research and Engineering Laboratory, 2021), http://dx.doi.org/10.21079/11681/42163, public domain. Additional portions have been modified and reprinted from M. F. Bigl, S. A. Beal, M. R. Walsh, C. A. Ramsey, and K. M. Burch, *Sieve Stack and Laser Diffraction Particle*

Size Analysis of IMX-104 Low-Order Detonation Particles, ERDC/CRREL TR-20-3 (Hanover, NH: U.S. Army Engineer Research and Development Center, Cold Regions Research and Engineering Laboratory, 2020), http://dx.doi.org/10.21079/11681/35515, public domain.

COL Teresa A. Schlosser was commander of ERDC, and Dr. David W. Pittman was the director.

This page intentionally left blank.

1 Introduction

1.1 Background

Military training with high explosives can deposit residual explosive solids on the surface of training ranges. Accumulation of these residues can have local ecological impacts, and dissolution of energetic compounds from these residues can infiltrate groundwater. Such environmental impacts have led to restrictions on training for some ranges and costly cleanup activities (Clausen et al. 2004; Racine et al. 1992; M. E. Walsh et al. 1996). Fully characterizing the sources of explosive residues is critical to the effective environmental management of ranges and the sustainment of military training and readiness.

Munitions containing conventional high explosives, such as 2,4,6-Trinitrotoluene (TNT) and Composition B (Comp B; a mixture of 1,3,5-Trinitro-1,3,5-Triazinane [RDX] and TNT), produce trace quantities of energetic residue (<10 mg* per round) when the munitions perform as intended in high-order (HO) detonations (Hewitt et al. 2005; M. R. Walsh et al. 2011). The primary sources of RDX and TNT on ranges are low-order (LO) detonations, which occur from munition malfunctioning and are characterized by the distribution of varyingly sized particles of unconsumed explosive filler (Jenkins et al. 2002). The physical particle characteristics (i.e., mass, size, composition, and morphology) and their spatial distribution from LO detonations are fundamental parameters in accurate estimation (i.e., fate and transport modeling) of environmental impacts to groundwater (Taylor et al. 2015). A nonfunctioning explosive munition, termed a *dud*, can release its entire energetic contents to the environment; however, this process likely occurs over much longer timescales (i.e., decades) due to slow corrosion of the metal casing (Chendorain and Stewart 2005).

Previous studies have used a variety of techniques for simulating LO detonation and characterizing produced particles. Taylor et al. (2006) and Pennington et al. (2008) used a combination of trays and tarpaulins to capture particles produced from LO detonations of mortar and artillery

* For a full list of the spelled-out forms of the units of measure used in this document and their conversions, please refer to *US Government Publishing Office Style Manual*, 31st ed. (Washington, DC: U.S Government Publishing Office, 2016), 245–252, https://www.govinfo.gov/content/pkg/GPO-STYLEMANUAL-2016/pdf/GPO-STYLEMANUAL-2016.pdf.

rounds, which were simulated using shaped charges positioned adjacent to the study munitions. The particles from these studies were characterized using sieving from >12.5 to <0.25 mm. As part of Strategic Environmental Research and Development Program (SERDP) ER-2219, LO detonations were initiated using small masses of C-4 plastic explosive in a fuze simulator that replaced the standard-issue fuze on 81 mm mortar rounds filled with IMX-104 (an insensitive munition formulation containing RDX, 3-nitro-1,2,4-triazol-5-one, and 2,4,-dinitroanisole; Bigl et al. 2020). These detonations were performed on bare ice; nearly all generated particles were collected in discrete annuli out to 20 m surrounding the point of detonation. Particles were isolated from entrained snow and ice by freeze drying; and, similar to the previous studies on tarps, the material was characterized using sieves from >9.51 to <0.5 mm.

The prior task of the project (Environmental Security Technology Certification Program [ESTCP] ER18-5105) demonstrated a complete method of characterizing LO-detonation particles by using 60 mm and 81 mm mortar rounds filled with IMX-104 (Bigl et al. 2021). This method used a fuze simulator to initiate LO detonations and bare ice as a sampling medium, combined with a complete particle-characterization suite and quality-control sampling approach. The important findings during the first part of this demonstration were (1) complexity in reproducible command LO detonation, (2) variability in fine-particle-size distributions elucidated by laser-diffraction particle-size analysis (LD-PSA), and (3) fine-fraction particle impurities for some samples. While this method was successfully demonstrated for IMX-104 mortar rounds, its efficacy on mortar rounds using the conventional explosive Comp B was not studied. Key differences in the sensitivity and optical properties between IMX-104 and Composition B require validation of each explosive through full method demonstration.

1.2 Objectives

The goal of this study was to demonstrate a method of purposefully initiating LO detonations and characterizing resulting residual explosive particles, specifically using high-explosive mortar rounds containing Comp B.

The specific demonstration objectives were

1. to successfully command detonate 81 mm Comp B mortar rounds LO;
2. to sample all of the resulting LO particles on clean ice in spatially resolved increments; and

3. to characterize LO particle samples for their size, composition, and morphology.

1.3 Approach

This study demonstrated a method of initiating LO detonation of 81 mm mortar rounds containing Comp B and comprehensively characterizing their produced residual explosive particles. An iterative approach to LO initiation using a variable-mass fuze simulator enabled successful LO detonation of the study munition. LO particles were sampled with high spatial resolution up to a radial distance of 20 m from the point of detonation. Explosive particles were isolated by freeze drying and sieving and then characterized using a suite of analytical techniques. In particular, the optical properties of Comp B were optimized and used to characterize fine-particle-size distributions by LD-PSA. Reproducibility, quality control, and process observations were used to assess method performance and broader applications.

2 Methods

2.1 Munitions

Munitions for testing were sourced through the Army Total Ammunition Management Information System and handled by the 716th Explosive Ordnance Disposal Company. The tested munition was the C868 M821 81 mm mortar rounds containing RDX and TNT filler. The 81 mm rounds consisted of two-part mortar bodies with full tail assembly and fuze. Prior to use in these tests, Explosive Ordnance Disposal removed the fuzes to be replaced by the CRREL Fuze Simulator (CFS) during testing.

2.2 Command detonations

LO detonations were performed by replacing the standard-issue fuze with the CFS containing a field-variable amount of C-4 and initiating with an electric blasting cap (M. R. Walsh et al. 2011). The command-detonation method used was identical to that of prior tests using IMX-104 rounds (Bigl et al. 2021), with the exception of the use of a pocket penetrometer to press the C-4 in the CFS to 8.7 psi to ensure consistency of C-4 packing (Figure 1).

Figure 1. Procedure of loading the CRREL Fuze Simulator (CFS) with C-4 for the low-order (LO) detonations.

Additionally, a C-4 punch was used prior to threading the CFS into the round to ensure the C-4 plug was not unseated during this process, and vinyl tape was put over the fuze well to keep the plug from being pushed into the supplemental-charge well during arming. Remote detonators were used with electrically initiated blasting caps and wire leads less than 5 m in length. Confirmation tests were conducted to determine the optimal mass of C-4 in the CFS to trigger a LO detonation. Prior to conducting command detonations, the supplemental charge and all propellant charges were removed (except for Charge 0 in the tail assemblies). The 81 mm mortar bodies were placed nose up for ease of arming the round with the blasting cap and on a 30 × 30 cm steel plate to reduce damage to the sampling area and to maintain integrity of the ice surface.

2.3 Field site and conditions

Tests were performed during February 2020 at the Eagle River Flats (ERF) Impact Area of Joint Base Elmendorf-Richardson (JBER) in Anchorage, Alaska. Snow was removed from the test area using a front-end loader and plow truck, and then smooth ice surfaces were created at several approximately 50 m diameter test sites by using a towed water trailer (Figure 2). On each day of testing, any freshly fallen snow was removed from the test sites through a combination of a backpack blower, squeegees, and push brooms. Temperatures during testing ranged between approximately –24°C and –6°C with minimal to no wind.

Figure 2. Preparations on the two primary testing sites.

2.4 Sampling design

At the center of the sampling area, each tested round was placed nose up on a 30 × 30 cm steel plate. Sampling annuli were marked with spray paint measured out from the point of detonation centered on the munition. The annuli were marked at 1 m intervals from 0 to 10 m and 5 m intervals from 10 to 20 m from the center (Figure 3).

Figure 3. Conceptual sampling design with annuli marked by dashed lines up to 20 m from the point of detonation.

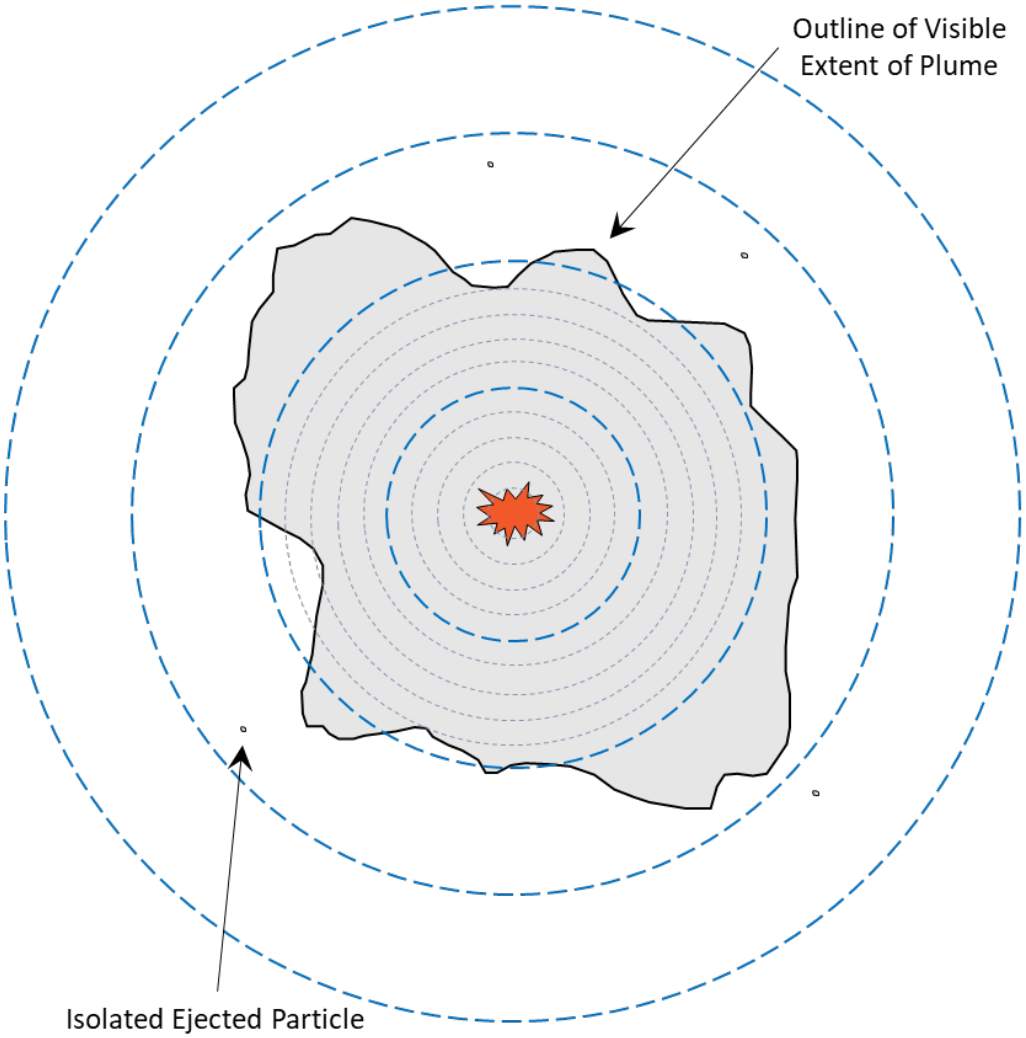

2.5 Sampling

Particles were collected into piles by carefully sweeping each annulus with push brooms without abrading the particles on the ice surface (Figure 4). The shank of a screwdriver was run repeatedly through the broom bristles to dislodge any particles retained within. Paint brushes and stainless-steel

drywall knives were used to transfer particles from the ice surface to large Whirl-Pak bags (Figure 4). Each Whirl-Pak bag was placed in its own zip-closed plastic bag to avoid cross contamination and any loss of sample in the event that the Whirl-Pak were to break or open. To minimize cross contamination, the push brooms used to sample the outer 10–15 m and 15–20 m annuli were kept separate from brooms used to sample the inner annuli. Between samples, push brooms and other sampling tools were cleaned by running the tool over or through clean snow; and between sampling days, they were cleaned with Micro-90 cleaning solution and left out in the heated lab to dry overnight.

Figure 4. Sampling teams sweeping the 10–15 m and 15–20 m annuli from sample 20FRA-L06 on the west test site.

2.6 Quality assurance / quality control

Background snow was sampled before testing to ensure the absence of preexisting energetic material at the testing area. *MULTI INCREMENT*® samples,* each composed of approximately 100 increments, were collected in triplicate from four background sites surrounding the testing area by

* *MULTI INCREMENT*® is a registered trademark of EnviroStat, Inc.

using a 10 × 10 × 2.5 cm scoop. Each background sample was melted in the laboratory on JBER and processed following the methodology of M. E. Walsh (2016), including filtration through a glass-fiber filter and solid-phase extraction of 500 mL of filtrate with a Waters PoraPak RDX cartridge. Samples were shipped to the Cold Regions Research and Engineering Laboratory (CRREL) in Hanover, New Hampshire, for analysis.

Following the collection of particles from select detonations, the entire sampling area was reswept into one sample and designated the postsample check to quantify the mass of energetic material missed after sweeping. As a secondary check, the entire sampling area was reswept again with a dedicated push broom into one sample and designated the postsample check verification. These quality-control samples were melted and filtered through glass-fiber filters at the laboratory on JBER, then shipped to CRREL for analysis.

Pre- and postfiltration blanks, blanks, matrix spikes, and laboratory control samples were also processed and analyzed at CRREL (Appendix A).

2.7 Particle isolation

Bagged samples from each annulus were transferred to 8 oz wide-mouth glass jars in a cold room at approximately –20°C. An unbleached coffee filter was placed on the opening of each jar and affixed by a plastic ring cap. Sample jars were placed inside 600 mL freeze-drying glass bulbs and connected to a VirTis Freezemobile 12XL at a set temperature of –75°C for 30–120 hr.

Freeze-dried samples were initially dry sieved at 2 mm, with oblong particles greater than 2 mm in any dimension removed manually with tweezers to avoid obstruction of the LD-PSA system. Visibly nonenergetic materials (i.e., metal fragments and vegetation) were manually removed with tweezers. The masses of the >2 mm and <2 mm size fractions were recorded prior to LD-PSA.

2.8 Particle-size analysis

Coarse particle sizes were determined on all samples by dry sieving the >2 mm fraction through 9.51, 4.75, and 2.83 mm sieves and recording the masses in each fraction. Only the fine fraction (<2 mm for most samples) was submitted to LD-PSA. However, the presence of long needles in some

samples prohibited their analysis by LD-PSA. For these samples, the <2 mm fraction was sieved through 0.5 and 1 mm sieves, and the masses in each fraction were recorded.

LD-PSA was performed on the <2 mm fraction of samples without needles and on the <0.5 mm fraction of two samples that had sieve-removable needles by using a Horiba LA-960 (Horiba Ltd., Kyoto, Japan). The configuration of this analyzer for the processing of energetic material is described in Bigl et al. (2020) and was not changed for the purposes of the analyses described below. The Horiba LA-960 was run on automatic feeder settings with the forced air pressure set to 0.03 MPa, a refractive index (RI) of $1.921 - 0.002i$, and sample data acquisition times of 50,000 counts (about 50 sec). The process of determining the RI for these particles was consistent with the methodology described in Bigl et al. (2020), and the results are described below. All samples required multiple analyses for the entirety of the sample material to pass through the analyzer during a measurement cycle. Following analysis, samples were recovered from the stainless-steel collection chamber of the Nilfisk 118EXP vacuum by using static-free brushes. To avoid cross contamination, Ottawa sand was run through the analyzer as a cleaning agent after each sample.

All of the samples had multiple output data files (each associated with an analysis of a fraction of the material), which required averaging. The volumetric percent for each analytical size fraction (0.011 µm to 5 mm) and the instrument-calculated D10, D50 (median), and D90 values were averaged for each sample. These values represent the particle size at which 10, 50, and 90 volume percent of the distribution falls under, respectively.

Samples that could not be run through the Horiba LA-960 due to needle-shaped particles, which clogged the instrumentation (described in Section 3.5), were analyzed using sieve-stack methods with bin sizes of 0–0.5 mm, 0.5–1 mm, and 1–2 mm, in addition to the larger bin sizes previously mentioned (Bigl et al. 2020). Bigl et al. (2020) outlined that LD-PSA is a more highly resolved analytical technique for energetic particle analysis; however, when that option is not feasible, sieve stack and particle-mass distribution serve as effective counterparts to LD-PSA.

2.9 Particle sample extraction

The chemical purity of the fine fraction was assessed using subsamples of <2 mm particles after LD-PSA or, if needle-shaped particles prohibited

LD-PSA, the <0.5 mm sieve fraction. Triplicate subsamples each consisted of approximately 200 mg of material collected in approximately 20 increments across the sample spread out in a thin layer on aluminum foil. Each subsample was extracted in a 2 oz glass jar using 30.0 mL of acetonitrile on a shaker table for 18 hr at 170 rpm. Extracts were syringe filtered at 0.45 µm (Millex FH), diluted 2000× with acetonitrile, and then mixed at a ratio of 1/3 with Type I water.

2.10 Chemical analysis

Chemical analysis was conducted using high-performance liquid chromatography (HPLC) following US Environmental Protection Agency (EPA) method 8330B (EPA 2006) on an Agilent 1260 Infinity II. The method used a Novapak C8 column (150 × 3.9 mm, 4 µm) and 15/85 (volume/volume) isopropanol/water mobile phase at 1.25 mL/min and 25°C. The target analytes were detected by UV absorption at 254 nm with retention times of 1.7 min for 1,3,5,7-tetranitro-1,3,5,7-tetrazocane (HMX), 3.4 min for RDX, and 6.1 min for TNT. Concentrations were quantified based on peak area and a seven-point external calibration (0.05 to 10 mg/L) using standards from Restek. Independent calibration verification used a separate lot standard from Restek (8095 Calibration Mix A).

Discrete subsamples of select <2 mm fractions were mounted on carbon adhesive tape, placed in a charge-reduction sample holder, and analyzed by a scanning electron microscope (SEM; Phenom ProX). Three samples from each sampled LO detonation were analyzed. Qualitative elemental composition was measured by energy dispersive x-ray spectroscopy (EDS) at 10 kV in point mode.

2.11 Morphological analysis

Select particle samples >2 mm were measured by microcomputed tomography (µCT) using a Bruker Skyscan. Using the Bruker system software, the three-dimensional sample reconstruction can be rotated 360° to observe detailed particle morphology. This technique reveals the complete structure of the particle, including crystalline components, porosity, and shape.

3 Results and Discussion

3.1 Command-detonation trials

No prior tests had been conducted with the M821 C868 81 mm round prior to this field season. Previous performance of the originally requested munition, M889A2 CA43 81 mm Comp B rounds, used 12 g of C-4 in the CFS to initiate an HO detonation (Walsh et al. 2018). Based on this performance, a minimum reduction in C-4 booster of 25% was used for initial LO command-detonation confirmation tests. This resulted in the selection of C-4 booster masses of 8 and 7 g for the first two confirmation tests, labeled 20FRA-CON1 and 20FRA-CON2, respectively. Table 1 summarizes all confirmation test sample IDs and visual inspection results. The confirmation test using a 7 g C-4 booster produced, by visual inspection, an HO detonation, characterized by only black residue remaining on the ice surface. During the 8 g confirmation test, the electric blasting cap did not initiate, and the round was reused for further testing. A third confirmation test, 20FRA-CON3, used an IMX-104 81 mm mortar round and a prior-optimized C-4 booster mass of 7.5 g to test whether the command-detonation setup was performing. This test resulted in a successful LO detonation, indicating a functioning system. For confirmation tests 4–8, the supplemental charge was removed, and booster masses were varied from 6 to 7 g.

Following the confirmation test of 20FRA-CON8, it was discovered that there was an environmental seal over the explosive filler that was not shown in the diagrams from the Army ammunition data sheets found in Technical Manual 43-0001-28 (US Army 2021). This seal had been left in place during earlier tests and was removed for the following two confirmation tests. Once the environmental seal was removed, both 20FRA-CON9 and 20FRA-CON10 resulted in LO detonations with approximately 6.5 g of C-4 booster. This booster mass was considered to produce a consistent LO result and was selected for testing the remaining rounds. Throughout all confirmation tests, the visual result of most rounds was an initiated dud with the round splitting at the nose cone (Figure 5). As mentioned earlier, the M821 C868 round consists of a two-part body design. The details of this design are such that the nose cone can be unthreaded to reveal the supplemental charge and the environmental seal below it. This was the method that was used to remove these items prior to rethreading the body of the round back together prior to testing.

Table 1. Visual test results and C-4 masses used in the CFS for 81 mm confirmation tests.

Round #	Site	C-4 (g)	Supplemental Charge	Env. Seal	Visual Result	Observations	Designation
1	Test Site 1	8.004	Yes	Yes	No Detonation	—	20FRA-CON1
2	Test Site 2	7.014	Yes	Yes	High Order	Black residue	20FRA-CON2
3	Test Site 1	6.001	No	Yes	Initiated Dud	Nose cone missing	20FRA-CON4
4	Test Site 2A	7.010	No	Yes	High Order	Black residue	20FRA-CON5
5	Test Site 1	6.489	No	Yes	Initiated Dud	Nose cone missing	20FRA-CON6
6	Test Site 1	6.460	No	Yes	Initiated Dud	Nose cone missing	20FRA-CON7
7	Test Site 1	6.751	No	Yes	Initiated Dud	Nose cone missing	20FRA-CON8
8	Test Site 1	6.497	No	No	Low Order	Visible powder/chunks	20FRA-CON9
9	Test Site 1A	6.503	No	No	Low Order	Visible powder	20FRA-CON10

Figure 5. An initiated dud from an attempted LO detonation of an 81 mm Composition B (Comp B) round.

After the confirmation tests described above, LO testing was conducted using the same initiation setup as 20FRA-CON9 and 20FRA-CON10. This consisted of removing both the supplemental charge as well as the environmental seal, using approximately 6.5–6.8 g of C-4 booster, which was prepared as described in Section 2.2. Table 2 summarizes the results of the LO-detonation testing. Four of the eight rounds tested detonated LO based on

visual inspection, with the remaining rounds resulting in partial detonations where the nose cone was liberated from the main body of the round. This was the primary result when rounds did not detonate LO and is described in more detail in Section 3.2. The four rounds that detonated LO were sampled either in bulk or in annuli. LO1 was sampled in bulk to provide material both for the RI estimation process and for a collaborative project.

Table 2. Visual test results and C-4 masses used in the CFS for 81 mm round LO tests.

Round #	C-4 (g)	Visual Result	Sampling Style	Designation
10	6.498	Low Order	Bulk	20FRA-LO1
11	6.503	Partial Detonation	Bulk	20FRA-LO2
12	6.608	Partial Detonation	Annuli	20FRA-LO3
13	6.655	Partial Detonation	—	20FRA-LO4
14	6.751	Partial Detonation	—	20FRA-LO5
15	6.850	Low Order	Annuli	20FRA-LO6
16	6.799	Low Order	Annuli	20FRA-LO7
17	6.804	Low Order	Annuli	20FRA-LO8

3.2 Physical observations from low-order detonations

Unlike HO detonations that usually deposit a dark black soot plume, the successful LO detonations shown in Figures 6–8 are clearly characterized by the scattering of light-colored particles with potentially some comingled darker-colored soot. The direction and extent of particle distribution appeared to vary between the LO tests. Particles from LO6 appeared to distribute relatively equally in all directions, whereas LO7 particles preferentially distributed in one direction and LO8 particles in two opposite directions. The clustering of particles in certain directions may reflect round-to-round differences in combustion propagation or in casing fracture.

Video stills from LO8 (Figure 9) provide visual clues into LO-detonation phenomena and particle distribution. Upon initiation, a bright central fireball was produced followed by secondary afterburning fireballs just above the ice surface. A large casing fragment was ejected greater than 20 m, and clusters of light-colored particles were formed and then deposited within approximately 10 m of the detonation. A cloud of fine light-colored material was produced and lingered above the testing site before dispersing and drifting out of frame. This fine material may have contained explosive particles but likely also was composed of condensed-phase postcombustion gases.

Figure 6. The 20FRA LO6 particle distribution prior to sampling.

Figure 7. The 20FRA LO7 particle distribution prior to sampling.

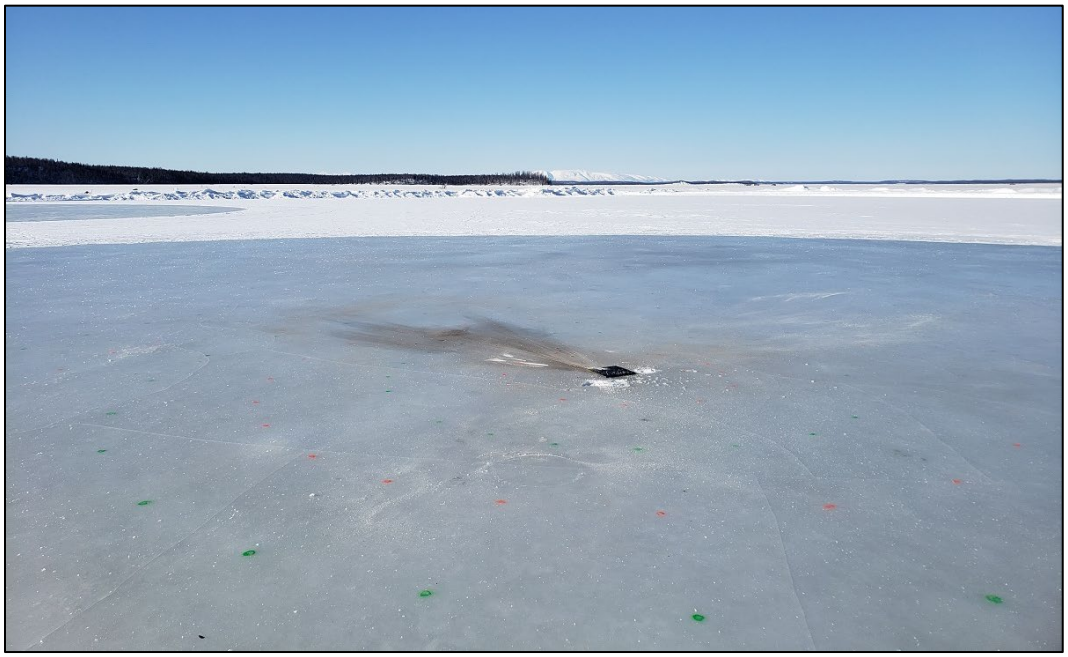

Figure 8. The 20FRA LO8 particle distribution during sampling.

Figure 9. Time sequence of the LO8 detonation. A wheel and tire were used to protect the remote detonator.

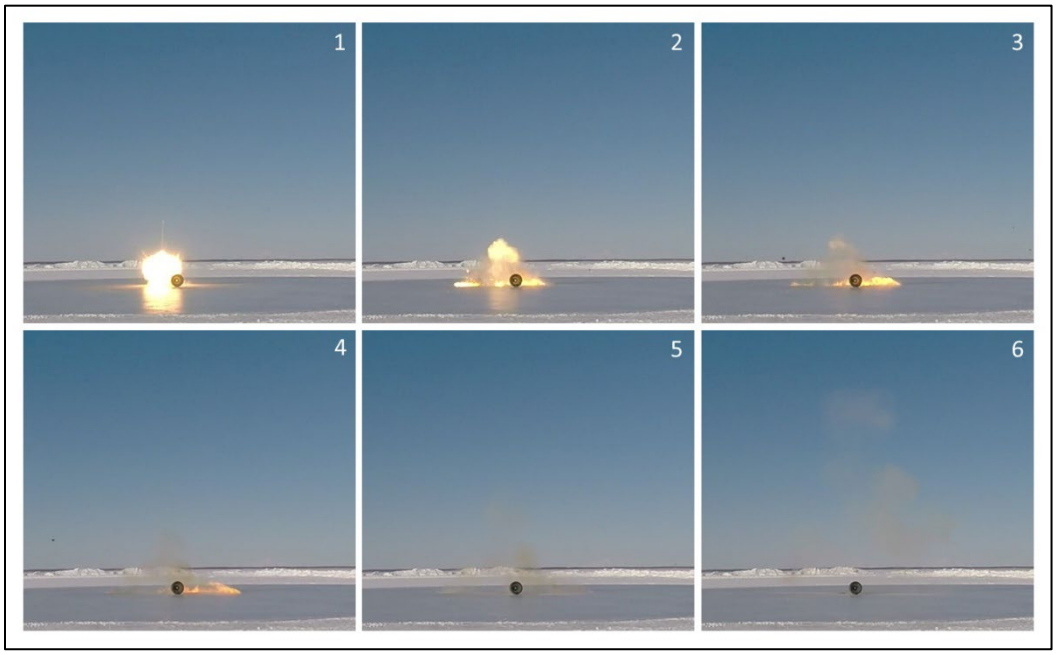

3.3 Quality assurance / quality control

All background samples had HMX, RDX, and TNT masses that were below the detection limit of approximately 0.001 mg (Appendix A, Table A-1).

The absence of these compounds provides strong evidence for pristine conditions at the testing sites prior to detonation.

Postsample checks and postsample check verifications after LO1 and LO8 provide estimates for the energetic mass not recovered during sampling. For LO1, only 0.9 g of energetics were collected during the postsample check and only 0.8 g during the postsample check verification (Table 3). Although samples from the LO1 detonation were not processed because of significant amounts of snow in the samples, these numbers suggest a high degree of recovery. For LO8, 19 g of energetics were collected from the postsample check and 5 g from the postsample check verification. The higher quantities during quality-assurance checks for LO8 indicate less complete recovery during sampling; however, they are similar in magnitude to quality-assurance checks during prior IMX-104 tests and may represent the practical recovery limit of the sampling method. While, altogether, these check masses are significantly lower than the sampled masses discussed below, which are on the order of hundreds of grams, they highlight the importance of interpreting the reported distributed particle masses as lower-limit estimates.

Table 3. Energetic masses from postsampling-sweep quality-control samples.

Sample	Aqueous (mg)			Solid (mg)			Total (g)
	HMX	RDX	TNT	HMX	RDX	TNT	
20FRA LO1 Postsample Check	<0.1	8.17	20.0	<0.2	543	310	0.882
20FRA LO1 Postsample Check Verification	<0.2	9.73	22.3	<0.2	482	244	0.758
20FRA LO8 Postsample Check	<0.1	29.5	68.7	<8	12900	5430	18.5
20FRA LO8 Postsample Check Verification	<0.1	20.7	52.2	<8	3620	1490	5.18

3.4 Sample composition

While nonenergetic particles could easily be removed from the large particle fraction of samples, purification prior to weighing of the fine fraction was not possible. Analysis of fine-fraction purity by dissolution and chemical analysis provides a robust measure of the energetic mass of the fine-fraction samples. Because of the large fine-fraction masses of some samples, the quantity of solvent needed to perform whole-sample extraction was prohibitive. Instead, triplicate subsamples of these fractions provided reproducible measures of particle purity (Figure 10 and Appendix B). Precision on subsamples was acceptable for all samples, with relative standard deviations ranging from 0% to 10% with an average of 3%.

For all sampled LO detonations, the fine fractions were relatively pure within 10 m of the center of the detonation (69%–99%) with an average of 91% for LO6, 82% for LO7, and 89% for LO8. Beyond 10 m, purity dropped precipitously for all detonations to as low as 11%. Possibly, the larger area of the 10–15 m and 15–20 m annuli provided more opportunity to incorporate foreign particles, or nonenergetic material from the detonation were preferentially distributed these distances.

Figure 10. Energetic composition (weight/weight) of the fine-fraction (<2 mm or <0.5 mm) samples after laser-diffraction particle-size analysis (LD-PSA) or sieving (not analyzed by LD-PSA). *Error bars* are plus or minus one standard deviation of triplicate subsamples.

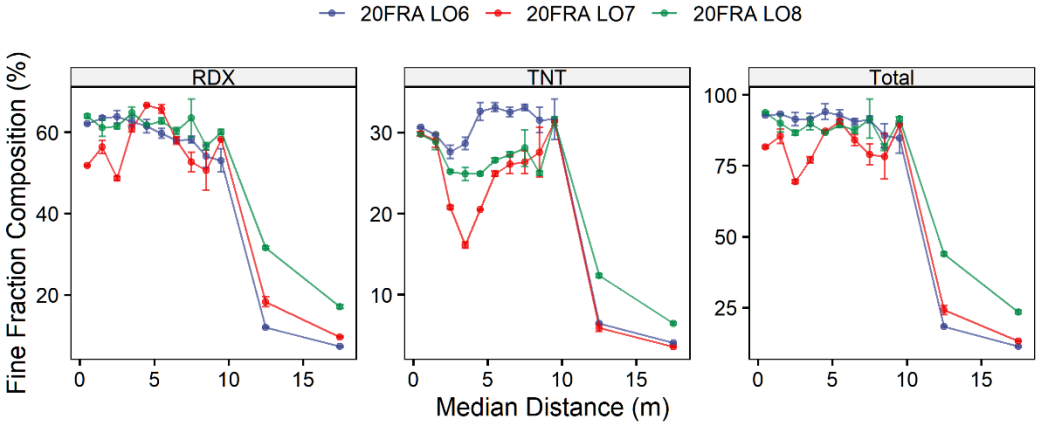

The quantitative measures of particle purity for each sample provide the means to correct the fine-fraction masses by using a purity factor. The main assumption with this correction is that the samples did not undergo fractionation during LD-PSA. The prior study of IMX-104 (Bigl et al. 2021) did observe some differences in particle composition between material collected in the LD-PSA vacuum filter and collection basin. In the present study, only the material collected in the basin was analyzed, as the finer material in the vacuum filter was difficult to remove and was more prone to run-to-run carryover.

3.5 Needles

The presence of elongated needle-shaped particles in many of the samples (Figure 11) prohibited their analysis by LD-PSA. The long, thin needles easily passed through 0.5 mm, 1 mm, and 2 mm sieves on their short axis and, if run through LD-PSA, would have clogged the light cell. To investigate the identity and origin of these needles, select needles were analyzed by SEM (Figure 12) and HPLC.

SEM-EDS measurements of the needle surface revealed a nitro-organic composition with approximately 36% carbon, 39% oxygen, and 22% nitrogen (weight/weight). Small particles on the exterior of the needles were composed of calcium carbonate. Needles selected for further testing dissolved rapidly in acetonitrile and had prominent HPLC peaks corresponding with TNT and nitroglycerin, with minor peaks corresponding with RDX and 2,4-dinitrotoluene. The TNT and RDX found in these needles were likely derived from fine adsorbed particles from the explosive filler, whereas the needles themselves likely were derived from the ignition cartridge composed primarily of nitroglycerin and nitrocellulose. Typical HPLC analysis does not reveal the latter compound. The ignition charges were not practicably removable from the tested munition, and these charges appear to have fractured during LO detonation of the round body.

Figure 11. Large needles separated from a LO Comp B sample. Smaller needles remained comingled with energetic particles in some samples and could not feasibly be removed.

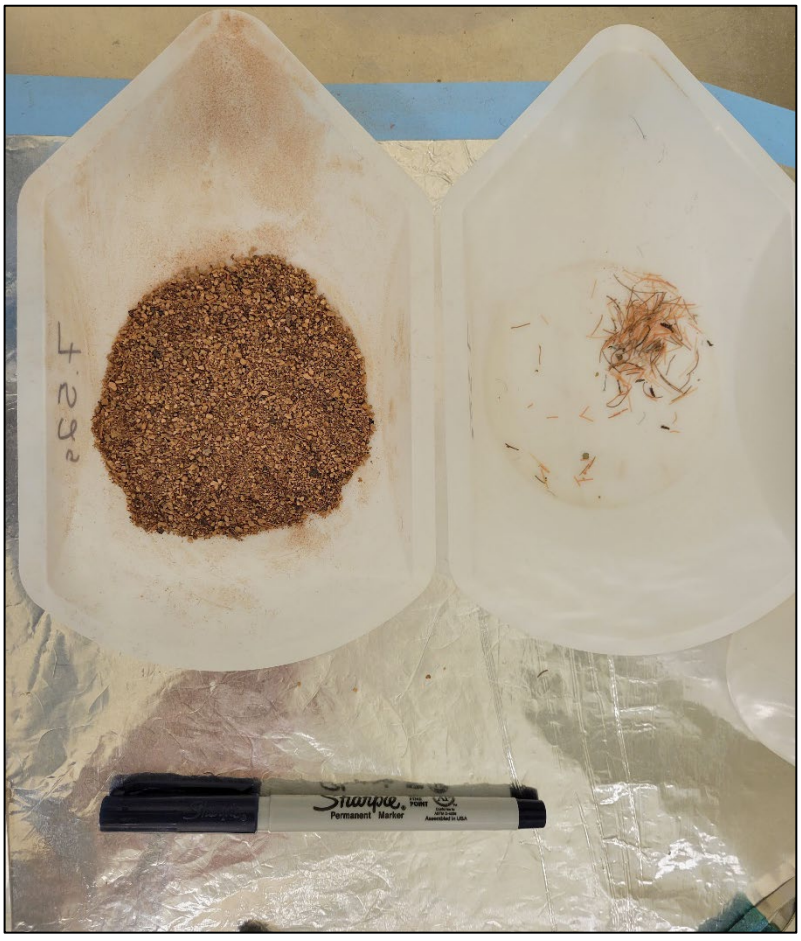

Figure 12. Scanning electron microscope image of a needle representative of those found in some LO-detonation samples.

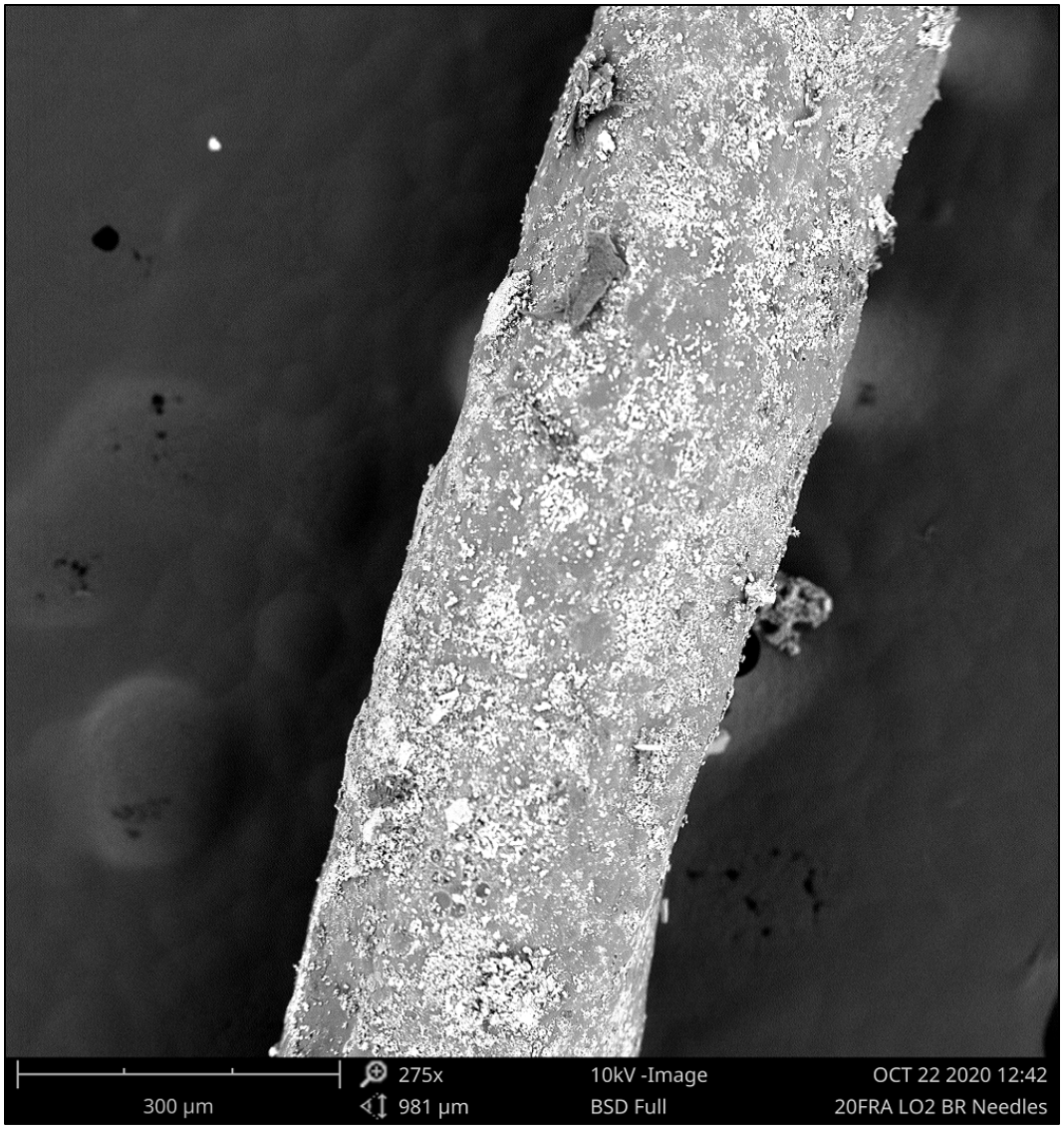

3.6 Refractive index estimation

As described in Bigl et al. (2020) the first step in estimating RI for an energetic material, in this case Comp B, is to analyze a single sample on the Horiba LA-960 and then recalculate the resulting particle-size distribution (PSD) estimation with new RI kernels while varying both the real and imaginary components. Bulk particles from LO1 were used for this estimation. Initially, the PSD was recalculated with a real component of 1, 2, 3, 4, and 5 and imaginary components for each of 0.01, 0.1, 1, 5, and 10. The resulting R parameters were then used to evaluate real and imaginary components over a wide range of values. This process allows for the

investigative window to be progressively narrowed by assessing the lowest nonzero R parameters within the range being evaluated. Table 4 summarizes the results of this first step.

Table 4. Summary of R parameter data for step one of the RI estimation for LO1 bulk particle analysis.

Real Component (*n*)	Imaginary Component (*k*)	R Parameter	Real Component (*n*)	Imaginary Component (*k*)	R Parameter
1	0.01	0.11811	4	0.01	0.0568
1	0.1	0.094262	4	0.1	0.057897
1	1	0.059475	4	1	0.059366
1	5	0.057828	4	5	0.059278
1	10	0.056737	4	10	0.057715
2	0.01	0.05555	5	0.01	0.05684
2	0.1	0.057137	5	0.1	0.057655
2	1	0.059549	5	1	0.058588
2	5	0.05775	5	5	0.058701
2	10	0.056765	5	10	0.057657
3	0.01	0.057805			
3	0.1	0.059681			
3	1	0.0598			
3	5	0.057744			
3	10	0.11811			

The lowest nonzero R parameter was returned for a real component of 2 and an imaginary component of 0.01 (Table 4). The second step of the RI determination process refined the imaginary component estimation by performing a recalculation of the original LO1 PSD with a fixed real component value of 2. For this step, the imaginary component values were varied from 0 to 0.1 in increments of 0.001 (Figure 13). The imaginary component with the lowest resulting R parameter was 0.002.

The third step in estimating the RI kernel was to fix the refined determined fixed imaginary component value of 0.01 and recalculate the R parameter for a range of real component values from 1.90 to 2.12 in increments of 0.01. The results of this recalculation determine the RI to the second decimal place (Figure 14). The lowest R parameter value was found for a RI real component of 1.92.

Figure 13. R parameters for fixed real component 2 and imaginary components ranging from 0 to 0.1

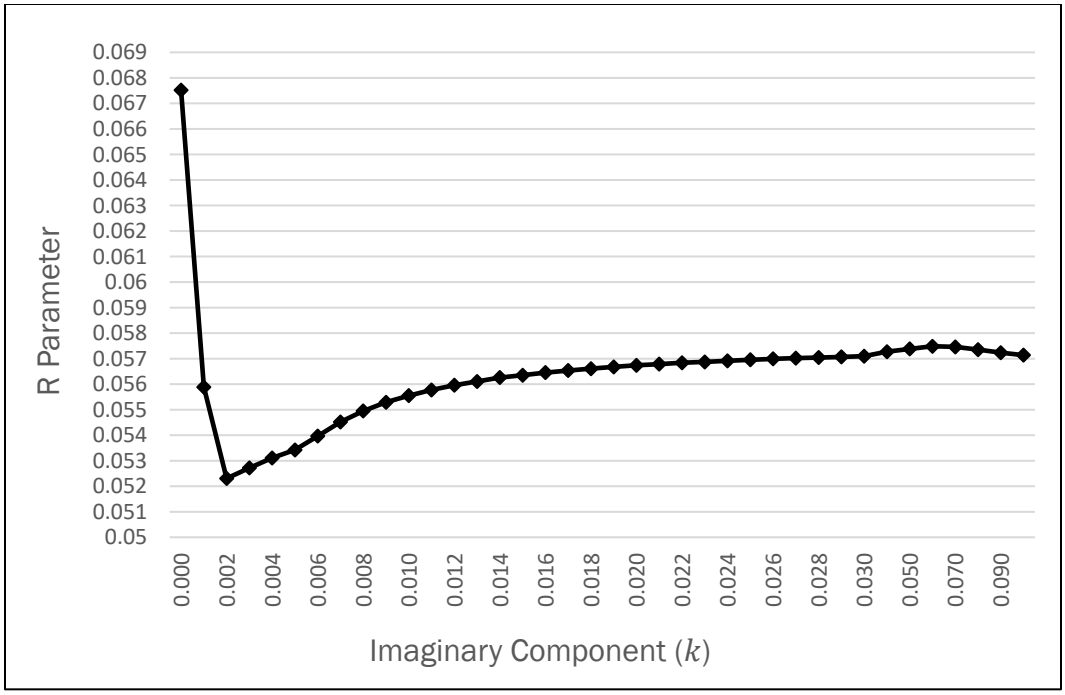

Figure 14. R parameters for refractive indices of 1.90–2.12 with a fixed imaginary component of 0.002.

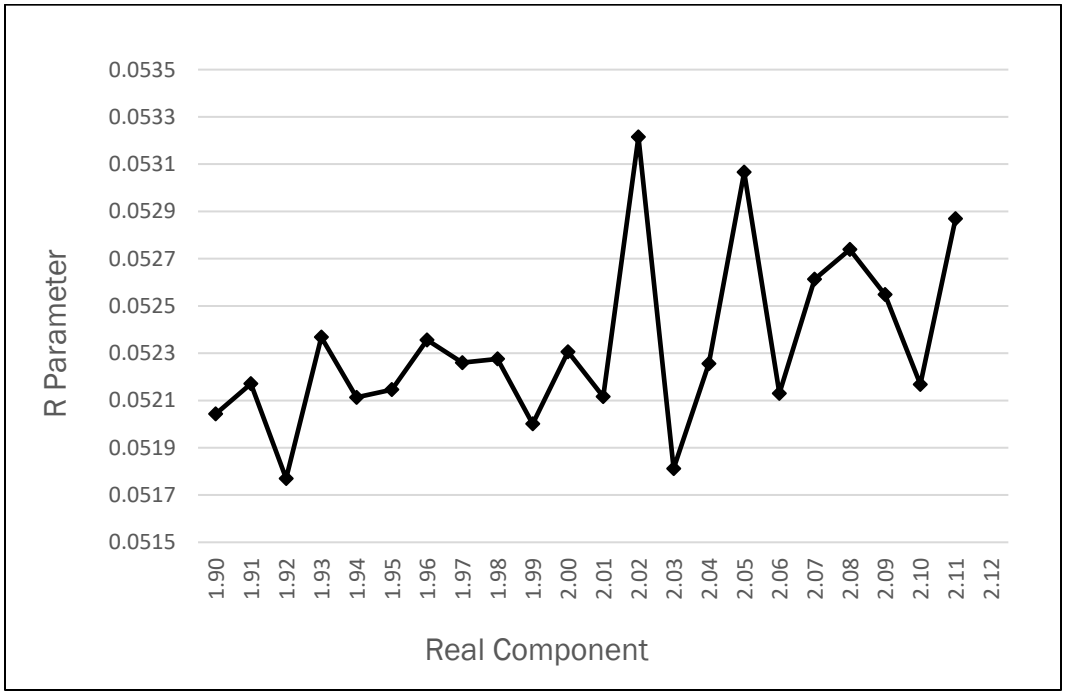

The fourth and final step determined the RI kernel to the third decimal place by holding the RI imaginary component constant at 0.002 and varying the real component from 1.890 to 1.938 in increments of 0.001 (Figure

15). This analysis yielded a real component of 1.921 with the lowest R parameter value.

Figure 15. Detail view of the lowest R parameter data for RI of 1.890–1.938 with a fixed imaginary component of 0.002.

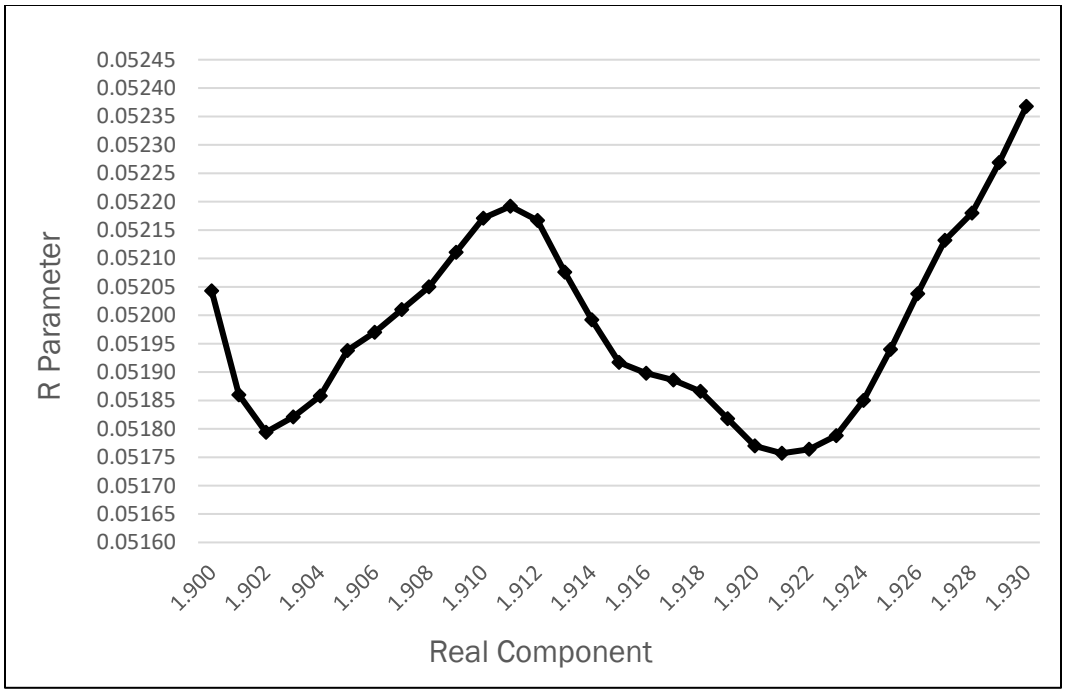

Through this four-step iterative process, the resulting RI kernel determined for Comp B was 1.921 (n) with an imaginary component (k) of 0.002, notated as $1.921 - 0.002i$.

3.7 Particle-mass distribution

Table 5 lists the particle-mass distribution by initial 2 mm sieve fraction for each sampling annulus. Particle masses in the fine fraction were corrected based upon HPLC energetic purity analyses, and masses in the coarse fraction were collected after removal of nonenergetic detritus. A detailed overview of this process is outlined in Bigl et al. (2021) for IMX-104 particles recovered from both 60 and 81 mm mortar rounds. Given the M821 C868 round has a predetonation energetic mass of 726 g, the total purity-corrected particle masses represent estimated consumption efficiencies of 68%, 82%, and 64% for LO6, LO7, and LO8, respectively. The <2 mm fraction dominates the total particle size for the majority of the sampled annuli, with only 5 of 36 sampled annuli having <2 mm fractions falling below 50% of total mass recovered. All five annuli in which this shift in dominant particle size occurs are within the 10–20 m range from

the point of detonation. The masses collected at distances greater than 20 m for LO7 and LO8 are predominantly for >2 mm large particles (Appendix D).

For LO6 and LO8, more than 45% of the total mass deposited was within 5 m from the point of detonation; however, for LO7, the deposition in the first 5 m represented only 25% of the total deposited mass. LO6 and LO8 had the highest per-meter depositional percentages within 5 m from the point of detonation with LO7 having the highest within the first 7 m from the point of detonation. Although LO6 and LO8 deposited a large amount of material within the first 5 m from the point of detonation, 47% and 57% respectively, significant amounts were also transported to the farthest annuli measured. All three detonations had high mass values (14–34 g) recorded in the 10–15 and 15–20 m annuli. However, these masses made up a greater overall percentage (42%) of deposition for LO7. The outer annuli mass deposition values need to be corrected from 5-radial-meter values to 1-radial-meter values to become comparable to the rest of the annuli (0–10 m). After doing so, there is an average deposition of 2.8–6.85 g per radial meter with the highest per-meter deposition resulting from LO6. These outer 5 m annuli account for 20.7%, 42.9%, and 17.5% of the total deposition for LO6, LO7, and LO8, respectively.

Table 5. The 2 mm purity-corrected sieve masses and mass proportions for 20FRA 81 mm samples.

Distance (m)	20FRA LO6			20FRA LO7			20FRA LO8		
	<2 mm (%)	>2 mm (%)	Total (g)	<2 mm (%)	>2 mm (%)	Total (g)	<2 mm (%)	>2 mm (%)	Total (g)
0–1	93.75	6.25	20.47	97.56	2.44	5.37	95.86	4.14	44.46
1–2	84.80	15.20	16.71	93.62	6.38	7.48	87.69	12.31	41.61
2–3	86.84	13.16	27.25	88.98	11.02	4.10	84.99	15.01	17.68
3–4	93.44	6.56	29.27	85.67	14.33	5.26	87.32	12.68	26.55
4–5	90.72	9.28	15.91	88.20	11.80	7.86	82.16	17.84	21.12
5–6	91.48	8.52	18.44	86.82	13.18	8.63	86.42	13.58	17.59
6–7	83.10	16.90	16.91	85.44	14.56	8.45	84.90	15.10	14.70
7–8	80.25	19.75	15.23	78.68	21.32	6.84	79.35	20.65	11.13
8–9	59.53	40.47	13.76	69.67	30.33	7.48	71.48	28.52	9.12
9–10	56.64	43.36	9.39	72.06	27.94	6.77	65.96	34.04	8.11
10–15	40.17	59.83	34.25	52.94	47.06	31.30	44.95	55.05	28.92
15–20	26.25	73.75	13.85	14.53	85.47	19.98	21.61	78.39	16.83
>20	—	—	—	—	—	9.28	—	—	3.91
Total	73.9	26.1	231	70.3	29.7	120	79.6	20.4	262

3.8 Particle-size distribution

Figure 16 shows the PSD data in percent by volume for <2 mm size fractions for all annuli samples without needle-shaped particles. The most complete LD-PSA sample set was for LO6. LO7 and LO8 had a significant quantity of needle-shaped particles that precluded them from LD-PSA analysis, so their sieve analysis will be described in the latter half of this section. For LO6, the farthest samples, 10–15 m and 15–20 m, also had a large amount of needles and were sieved to <0.5 mm prior to LD-PSA analysis. These samples will be presented separately from the <2 mm samples to avoid comparing and drawing conclusions from two separate size fractions. For LO6, there were broad bimodal peaks of varying size for the 0–4 m annuli. The 4–10 m annuli for LO6 had larger peaks associated with coarser particle sizes with small shoulder peaks representing the finer material. The farthest annuli (10–20 m) for LO6 can be characterized as broad peaks centered over approximately 100 μm. The only annuli that could be analyzed by LD-PSA for LO7 were 7–8, 8–9, and 9–10 m. All three of these annuli had PSDs with sharp peaks centered over about 1 mm with either a coarser shoulder peak or a broad fine tail. The only annuli that could be analyzed for LO8 were 0–1, 1–2, and 9–10 m. As shown in Figure 16, the annuli closer to the point of detonation (0–2 m) have PSDs with short, broad peaks centered over approximately 500 μm. The PSD for the 9–10 m annulus has one sharp, tall peak centered over about 1 mm.

As described above, a significant portion of material from LO7 and LO8 needed to be analyzed by sieve stack as opposed to LD-PSA due to the presence of needle-shaped particles that would clog the Horiba LA-960. The PSDs in Figure 17 show the data in cumulative percent by mass and sampling annulus for LO7 and LO8. What is clearly evident from these plots is that a high proportion of fine material is found close to the detonation and general coarsening with increasing distance from the point of detonation. However, the majority of the material by mass is still <2 mm in size, as depicted in Figure 17 and Table 6. The <0.5 mm size fraction becomes a much less dominant size fraction with increasing distance from the point of detonation. Both LO7 and LO8 show this trend in reduction of fine-material deposition with increasing distance from the point of detonation.

The particle-size measurements D10, D50, and D90 provide an alternate method of examining changes in PSD with distance (Tables 6–9). As Table 6 shows, the highest values are observed 5–10 m from the point of detonation for LO6. This indicates that material becomes coarser the farther you

get from the point of detonation. Tables 8 and 9 cannot be interpreted with as much detail as Table 6 as they represent only three annuli each for both LO7 and LO8, respectively. From the small amount of data that is available for LO7 and LO8, it is clear that the samples become coarser with increased distance from the point of detonation.

Figure 16. Particle-size distributions (PSDs) from 81 mm Comp B LO detonations at Eagle River Flats. Certain annuli needed to be processed by sieve instead of LD-PSA and are shown in Fig. 17.

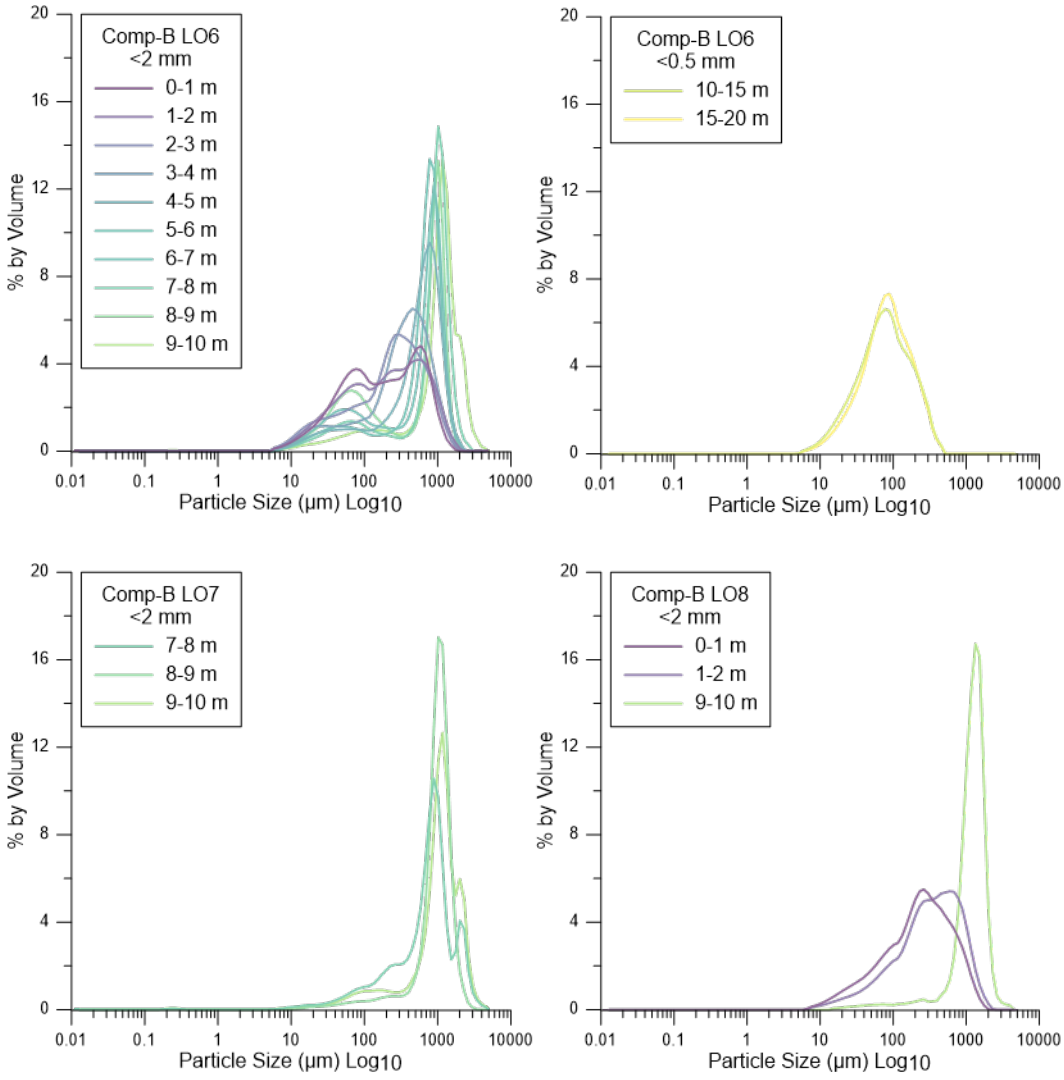

Figure 17. Cumulative percent mass PSDs using purity-corrected mass values from 81 mm Comp B detonations at Eagle River Flats.

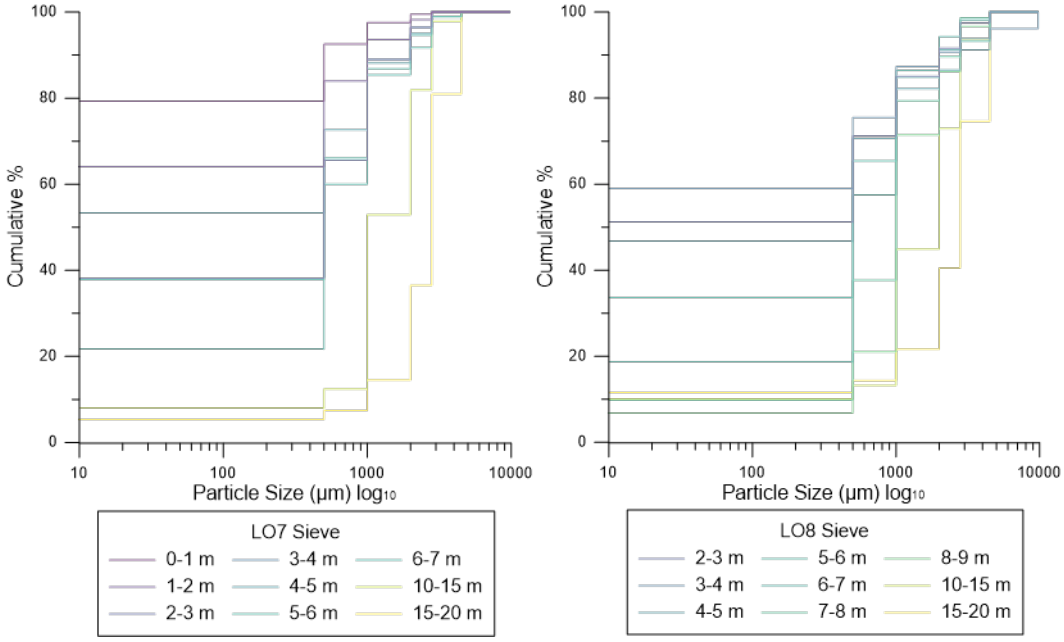

Table 6. Particle-size metrics for the 20FRA LO6 <2 mm fraction averaged for multiple analyses by LD-PSA.

Distance (m)	D10 (µm)	D50 (µm)	D90 (µm)
0–1	30	165	682
1–2	28	193	784
2–3	26	232	721
3–4	37	316	789
4–5	91	551	1025
5–6	85	650	1031
6–7	38	615	1091
7–8	130	820	1307
8–9	36	645	1104
9–10	232	1147	1666

Table 7. Particle-size metrics for the 20FRA LO6 <0.5 mm fraction averaged for multiple analyses by LD-PSA.

Distance (m)	D10 (µm)	D50 (µm)	D90 (µm)
10–15	22	71	205
15–20	25	77	201

Table 8. Particle-size metrics for the 20FRA LO7 <2 mm fraction averaged for multiple analyses by LD-PSA.

Distance (m)	D10 (µm)	D50 (µm)	D90 (µm)
7–8	206	877	1372
8–9	430	967	1403
9–10	347	1165	1670

Table 9. Particle-size metrics for the 20FRA LO8 <2 mm fraction averaged for multiple analyses by LD-PSA.

Distance (m)	D10 (µm)	D50 (µm)	D90 (µm)
0–1	30	165	682
1–2	28	193	784
9–10	232	1147	1666

3.9 Particle morphology

Figures 18 through 20 show µCT images taken of several >2 mm particles from 20FRA LO6, LO7, and LO8. The annulus in which these particles were sampled from varies for each detonation; however, some of the characteristics exhibited are consistent across all three samples. Brighter crystals of RDX are observed within a darker matrix composed of TNT. Figure 18 shows a three-dimensional reconstructed cross section of a particle sampled from the 5–6 m annuli of LO6.

Figure 18. A µCT image from 20FRA LO6 5–6 m.

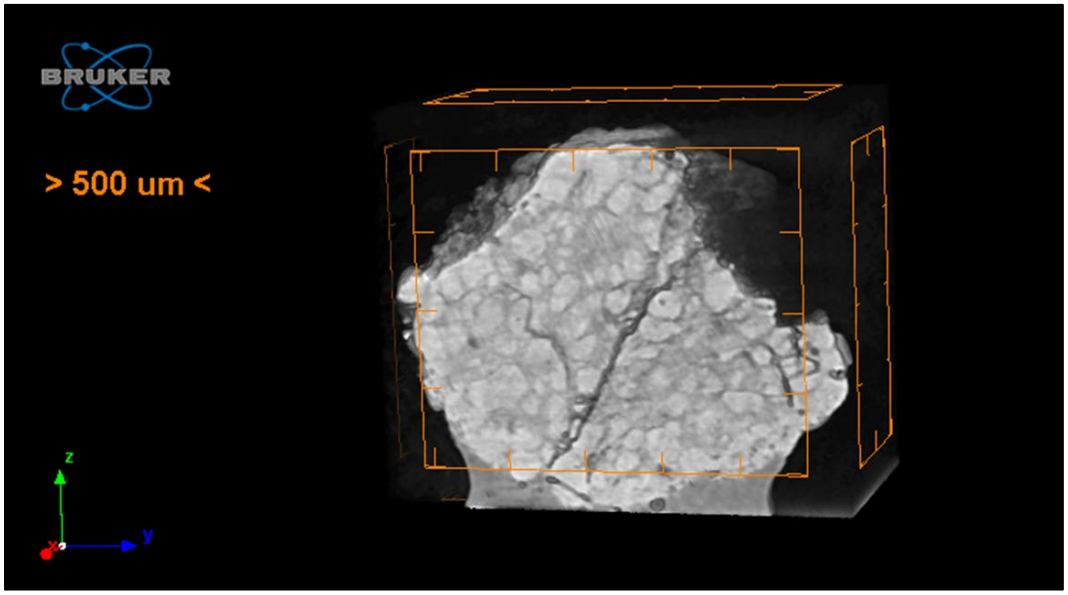

Figure 19. A µCT image from 20FRA LO7 2–3 m.

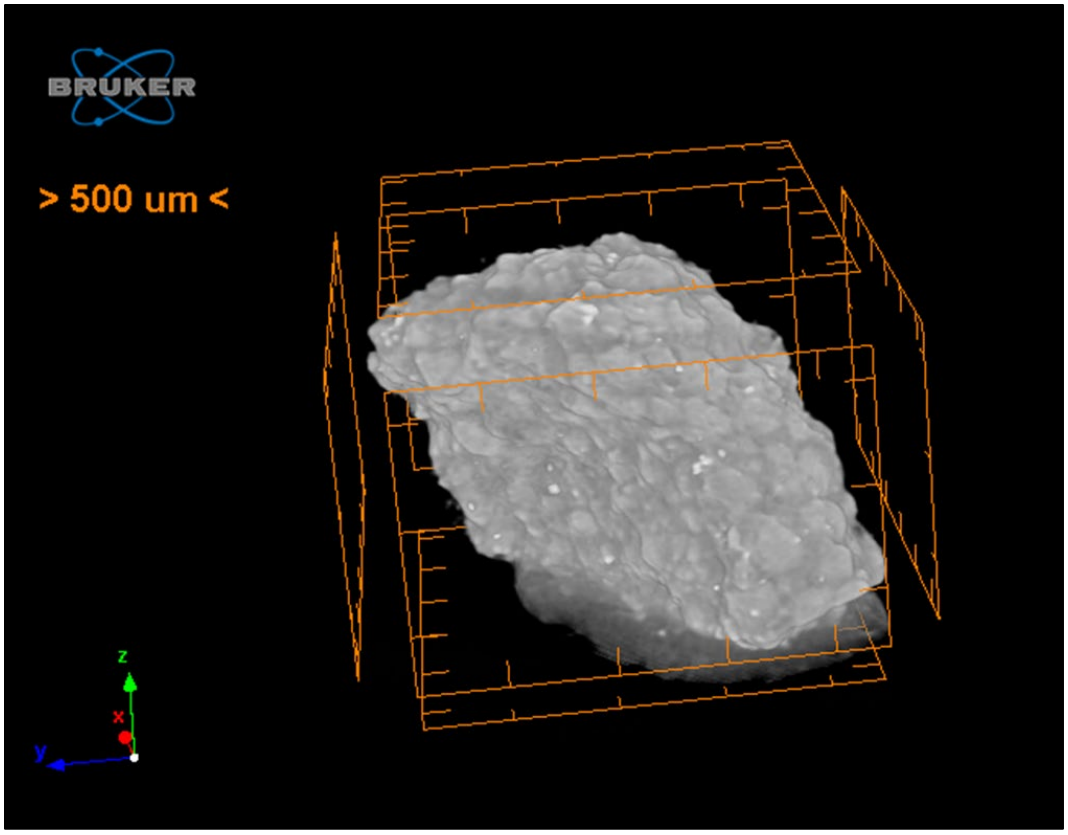

Figure 20. A µCT image from 20FRA LO8 2–3 m.

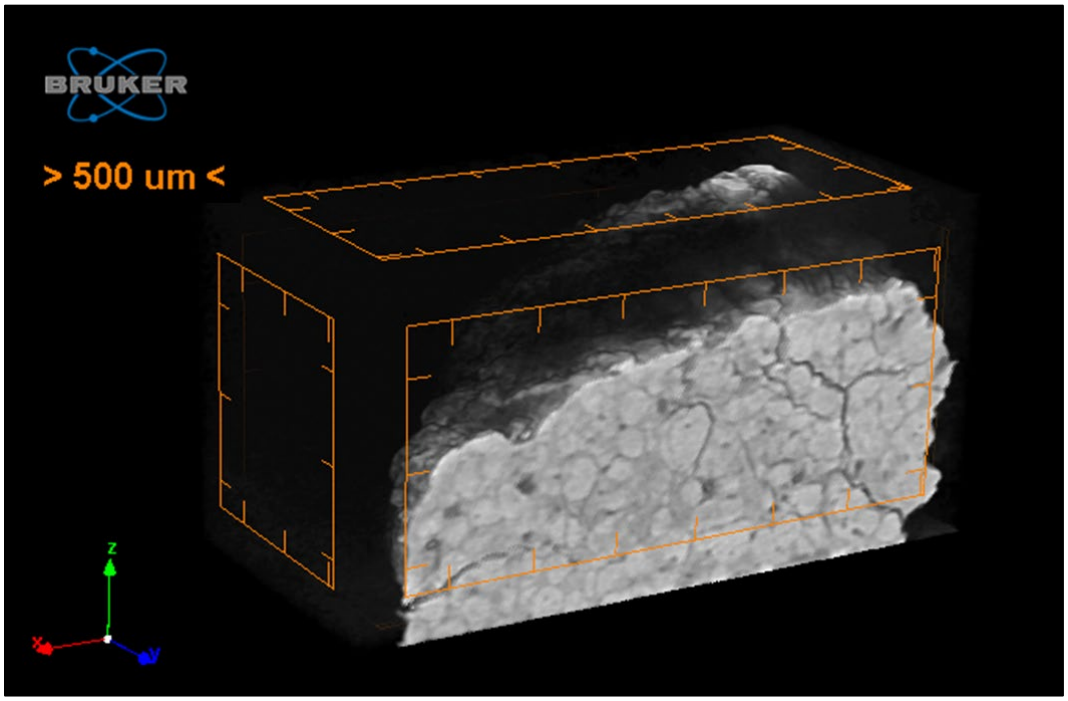

An irregular particle shape as well as several fractures of varying degrees throughout the particle are exhibited in the μCT scans. There is a main fracture through the center with several smaller distal fractures moving outward from this primary fracture and along the upper right edge of the particle. These fractures appear to propagate through the darker TNT matrix between lighter RDX crystals. This can then be compared to the two particles sampled from the 2–3 m annuli for LO7 and LO8, shown in Figures 19 and 20, respectively. Both of these particles are also irregular in shape; and, as seen in the cross section in Figure 18, there is also significant fracturing through the interior of the particle. In Figures 18 and 20, dark spots are clearly evident on the cross-sectional face of the particle. These could potentially be indicators of voids within the particle. The larger and darker spots tend to occur close to fractures or the exterior surface of the particle. The cause of these potential voids is unknown from the analytical results presented here; however, their presence in the results of this technique underlines the usefulness of analyzing particle morphology in this manner.

4 Conclusions

From observations made during attempted LO detonations using a fuze simulator, M. R. Walsh et al. (2017) proposed a classification scheme for munition detonation types based on the amount of explosive filler consumed and the condition of the munition following detonation (Table 10). The consumption efficiencies observed for the studied Comp B LO detonations described here would place LO7 (82%) as "Low Order" following this scheme; however, LO6 (68%) and LO8 (64%) would be classified as "Partial Detonations." Since the method provides a minimum estimate of particle mass, the actual consumption efficiencies are very likely lower than represented. Although there are clearly distinct modes of detonation based on the confirmation testing, the actual filler consumption efficiencies appear to vary widely within the LO-detonation mode.

Table 10. Classification of detonation order based on energetic mass recovered. (Table adapted from M. R. Walsh et al. 2017).

Detonation Type	Filler Mass Consumed (%)	Munition State
High Order	≥99.99	Total fragmentation of projectile body. Very fine residues (soot).
Low Order	75–99.98	Incomplete body fragmentation. Energetics particles on the ground and adhered to larger metal fragments.
Partial	25–75	Little if any fragmentation of the body. Large chunks of explosive filler (greater than centimeters in size).
Initiated Dud	<25	Fuze initiated. Mostly intact round. Adjacent loose chunks of explosive filler possible.
Noninitiated Dud	0	Round intact, including fuze. No ejection of explosive filler.

The successful execution of this demonstration provided novel fate-controlling particle characteristics for one type of conventional munition. The observed variability, spatial extent, and particle-distribution data can constrain LO-detonation inputs for this munition type in fate and transport models.

Command detonation was fully successful for the 81 mm rounds, even though confirming the LO testing setup for a completely new type of round proved difficult and time-consuming in the field. The two-part body design of the round used also proved to be problematic when approaching the lower limit of round performance. This additional point of failure increased the likelihood of a partial detonation resulting from the LO setup.

The additional refinements made to the CFS LO testing setup included consistent and measurable C-4 packing; punching the booster prior to assembly; and using tape underneath the booster cup, which proved to be helpful in narrowing the range of LO confirmation variables to be altered.

As reported in Bigl et al. (2021), when testing IMX-104 mortar rounds, ice conditions played a critical role in the ease and likely effectiveness of particle collection. Bumps, cracks in the ice, and residual snow can prevent particles from being collected, leading the reported mass distributions to serve as minimum estimates. The postsample check and postsample check verification provided quantitative estimates of the unrecovered particle mass during sampling. Flooding the sample site repeatedly with water during prep and testing was effective at creating a relatively smooth ice surface although imperfections were still present.

The observed shot-to-shot variability underlines the need to collect more replicate detonations when performing these types of tests. Increased replicate counts could provide more precise bounds on the variability of particle deposition within the range of LO-detonation efficiencies and, therefore, the patterns of deposition overall.

The presence of needle-shaped particles in the majority of annuli samples underlines the need to make use of all available measurement techniques when performing these types of characterizations. No single technique alone will provide the full picture of how material is distributed from LO detonations, and the ability to be flexible with analyses and interpretation is important. The success of performing RI estimation on Comp B particles demonstrates that the LD-PSA technique can be applied with relative ease to both insensitive (Bigl et al. 2021) and conventional explosive fillers. Repeatable testing on a modern particle-size analyzer still requires some adjustment to avoid undue sample loss and to ensure consistency across replicates; however, the application of this technique to explosive filler is still new, and further refinement is expected.

Overall, applying LD-PSA to particles of conventional explosive fillers greatly increases the resolution at which the deposition of this material can be understood on training ranges. Continued work to improve this approach, specifically for the analysis of particles that are an extremely irregular shape, such as the needle-shaped particles described herein, will further increase the effectiveness of this method. The better understanding

of the deposition of postdetonation material on training ranges that this method creates will improve fate and transport models, essential for the continued management of training lands.

References

Bigl, M. F., S. A. Beal, and C. A., Ramsey. 2021. *Determination of Residual Low-Order Detonation Particle Characteristics from IMX-104 Mortar Rounds*. ERDC/CRREL TR-21-12. Hanover, NH: US Army Engineer Research and Development Center, Cold Regions Research and Engineering Laboratory. http://dx.doi.org/10.21079/11681/42163.

Bigl, M. F., S. A. Beal, M. R. Walsh, C. A., Ramsey, and K. A. Burch. 2020. *Sieve Stack and Laser Diffraction Particle Size Analysis of IMX-104 Low-Order Detonation Particles*. ERDC/CRREL TR-20-3. Hanover, NH: US Army Engineer Research and Development Center, Cold Regions Research and Engineering Laboratory. http://dx.doi.org/10.21079/11681/35515.

Chendorain, M., and L. D. Stewart. 2005. "Corrosion of Unexploded Ordnance in Soil—Field Results." *Environmental Science and Technology* 39 (8): 2442–2447. https://doi.org/10.1021/es049300x.

Clausen, J. L., J. Robb, D. Curry, and N. Korte. 2004. "A Case Study of Contaminants on Military Ranges: Camp Edwards, Massachusetts, USA." *Environmental Pollution* 129 (1): 13–24. https://doi.org/10.1016/j.envpol.2003.10.002.

EPA (US Environmental Protection Agency). 2006. *Nitroaromatics, Nitramines, and Nitrate Esters by High Performance Liquid Chromatography (HPLC)*. Method 8330B. Washington, DC: US Environmental Protection Agency. https://www.epa.gov/sites/default/files/2015-07/documents/epa-8330b.pdf.

Hewitt, A. D., T. F. Jenkins, M. E. Walsh, M. R. Walsh, and S. Taylor. 2005. "RDX and TNT Residues from Live-Fire and Blow-in-Place Detonations." *Chemosphere* 61 (6): 888–894. https://doi.org/10.1016/j.chemosphere.2005.04.058.

Jenkins, T. F., M. E. Walsh, P. H. Miyares, A. D. Hewitt, N. H. Collins, and T. A. Ranney. 2002. "Use of Snow-Covered Ranges to Estimate Explosives Residues from High-Order Detonations of Army Munitions." *Thermochimica Acta* 384 (1–2): 173–185. https://doi.org/10.1016/S0040-6031(01)00803-6.

Pennington, J. C., B. Silverblatt, K. Poe, C. A. Hayes, and S. Yost. 2008. "Explosive Residues from Low-Order Detonations of Heavy Artillery and Mortar Rounds." *Soil and Sediment Contamination* 17 (5): 533–546. https://doi.org/10.1080/15320380802306669.

Racine, C. H., M. E. Walsh, B. D. Roebuck, C. M. Collins, D. J. Calkins, L. R. Reitsma, P. Buchli, and G. Goldfarb. 1992. "White Phosphorus Poisoning of Waterfowl in an Alaskan Salt Marsh." *Journal of Wildlife Diseases* 28 (4): 669–673. https://doi.org/10.7589/0090-3558-28.4.669.

Taylor, S., E. Campbell, L. Perovich, J. Lever, and J. Pennington. 2006. "Characteristics of Composition B Particles from Blow-in-Place Detonations." *Chemosphere* 65 (8): 1405–1413. https://doi.org/10.1016/j.chemosphere.2006.03.077.

Taylor, S., E. Park, K. Bullion, and K. Dontsova. 2015. "Dissolution of Three Insensitive Munitions Formulations." *Chemosphere* 119:342–348. https://doi.org/10.1016/j.chemosphere.2014.06.050.

US Army. 2021. *Army Ammunition Data Sheets for Artillery Ammunition: Guns, Howitzers, Mortars, Recoilless Rifles, Grenade Launchers and Artillery Fuzes (Federal Supply Class 1310, 1315, 1320, 1390)*. TM 43-0001-28. Washington, DC: US Army.

Walsh, M. E. 2016. "Analytical Methods for Detonation Residues of Insensitive Munitions." *Journal of Energetic Materials* 34:76–91. https://doi.org/10.1080/07370652.2014.999173.

Walsh, M. E., C. M. Collins, and C. H. Racine. 1996. "Persistence of White Phosphorus (P4) Particles in Salt Marsh Sediments." *Environmental Toxicology and Chemistry* 15 (6): 846–855. https://doi.org/10.1002/etc.5620150605.

Walsh, M. R., M. F. Bigl, M. E. Walsh, E. T. Wrobel, D. L. Zaloga, S. A. Beal, and T. Temple. 2018. "Physical Simulation of Live-Fire Detonations Using Command-Detonation Fuzing." *Propellants Explosives Pyrotechnics* 43:602–608. https://doi.org/10.1002/prep.201700316.

Walsh, M. R., T. Temple, M. F. Bigl, S. F. Tshabalala, N. Mai, and M. Ladyman. 2017. "Investigation of Energetic Particle Distribution from High-Order Detonations of Munitions." *Propellants, Explosives, Pyrotechnics* 42 (8):932–941. https://doi.org/10.1002/prep.201700089.

Walsh, M. R., S. Thiboutot, M. E. Walsh, G. Ampleman, R. Martel, I. Poulin, and S. Taylor. 2011. *Characterization and Fate of Gun and Rocket Propellant Residues on Testing and Training Ranges: Final Report*. ERDC/CRREL TR-11-13. Hanover, NH: US Army Engineer Research and Development Center, Cold Regions Research and Engineering Laboratory. http://hdl.handle.net/11681/5515.

Appendix A: Quality-Control Data

Table A-1. Prefiltering glassware method blanks, postfiltering method blanks, and background sample masses. Background samples are the average of triplicate *MULTI INCREMENT* samples. (*DNT* is *dinitrotoluene*; *Am* is *amino*.)

Sample	Total (mg)						
	HMX	RDX	TNT	2,4-DNT	2,6-DNT	2Am-DNT	4Am-DNT
Pre-Filter Blank 1	<0.0004	<0.0004	0.0005	<0.0004	<0.0004	<0.0004	<0.0004
Pre-Filter Blank 2	<0.0004	<0.0004	<0.0004	<0.0004	<0.0004	<0.0004	<0.0004
Post-Filter Blank 1	<0.0004	<0.0004	0.0005	<0.0004	<0.0004	<0.0004	<0.0004
Post-Filter Blank 2	<0.0004	<0.0004	<0.0004	<0.0004	<0.0004	<0.0004	<0.0004
20FRA BG #1	<0.001	<0.001	<0.001	<0.001	<0.001	<0.001	<0.001
20FRA BG #2	<0.001	<0.001	<0.001	<0.001	<0.001	<0.001	<0.001
20FRA BG #3	<0.001	<0.001	<0.001	<0.001	<0.001	<0.001	<0.001
20FRA BG #4	<0.001	<0.001	<0.001	<0.001	<0.001	<0.001	<0.001

Table A-2. Solid-phase-extraction matrix spike (MS), matrix spike duplicate (MSD), and laboratory control samples (LCS) each spiked at 4 µg/L with HMX, RDX, and TNT.

Sample	Recovery (%)		
	HMX	RDX	TNT
20FRA Background 4 MS	105	103	105
20FRA Background 4 MSD	100	100	101
LCS-1	123	120	120
LCS-2	124	120	127

Appendix B: Energetic Purity Data

Table B-1. Energetic composition for the fine fraction of LO6 samples. Values are presented as the mean plus or minus one standard deviation of triplicate subsample measurements.

Distance	Fraction	Weight Percent	
		RDX	TNT
0–1 m	<2 mm	0.621 ± 0.003	0.306 ± 0.001
1–2 m	<2 mm	0.634 ± 0.004	0.297 ± 0.001
2–3 m	<2 mm	0.638 ± 0.016	0.276 ± 0.008
3–4 m	<2 mm	0.627 ± 0.013	0.286 ± 0.008
4–5 m	<2 mm	0.615 ± 0.017	0.326 ± 0.011
5–6 m	<2 mm	0.597 ± 0.012	0.331 ± 0.006
6–7 m	<2 mm	0.580 ± 0.007	0.325 ± 0.006
7–8 m	<2 mm	0.582 ± 0.009	0.331 ± 0.004
8–9 m	<2 mm	0.540 ± 0.027	0.315 ± 0.016
9–10 m	<2 mm	0.530 ± 0.028	0.316 ± 0.025
10–15 m	<0.5 mm	0.119 ± 0.002	0.065 ± 0.001
15–20 m	<0.5 mm	0.073 ± 0.002	0.040 ± 0.001

Table B-2. Energetic composition for the fine fraction of LO7 samples. Values are presented as the mean plus or minus one standard deviation of triplicate subsample measurements.

Distance	Fraction	Weight Percent	
		RDX	TNT
0–1 m	<0.5 mm	0.517 ± 0.003	0.298 ± 0.002
1–2 m	<0.5 mm	0.564 ± 0.017	0.290 ± 0.009
2–3 m	<0.5 mm	0.486 ± 0.006	0.208 ± 0.002
3–4 m	<0.5 mm	0.609 ± 0.009	0.161 ± 0.004
4–5 m	<0.5 mm	0.666 ± 0.003	0.205 ± 0.000
5–6 m	<0.5 mm	0.656 ± 0.011	0.249 ± 0.004
6–7 m	<0.5 mm	0.579 ± 0.010	0.261 ± 0.011
7–8 m	<2 mm	0.527 ± 0.024	0.263 ± 0.014
8–9 m	<2 mm	0.507 ± 0.049	0.276 ± 0.031
9–10 m	<2 mm	0.582 ± 0.002	0.313 ± 0.001
10–15 m	<0.5 mm	0.182 ± 0.012	0.059 ± 0.004
15–20 m	<0.5 mm	0.096 ± 0.002	0.036 ± 0.000

Table B-3. Energetic composition for the fine fraction of L08 samples. Values are presented as the mean plus or minus one standard deviation of triplicate subsample measurements.

Distance	Fraction	Weight Percent	
		RDX	TNT
0–1 m	<2 mm	0.639 ± 0.004	0.298 ± 0.002
1–2 m	<2 mm	0.611 ± 0.022	0.288 ± 0.010
2–3 m	<0.5 mm	0.614 ± 0.006	0.252 ± 0.001
3–4 m	<0.5 mm	0.648 ± 0.013	0.249 ± 0.008
4–5 m	<0.5 mm	0.617 ± 0.003	0.249 ± 0.002
5–6 m	<0.5 mm	0.627 ± 0.008	0.266 ± 0.003
6–7 m	<0.5 mm	0.602 ± 0.009	0.273 ± 0.003
7–8 m	<0.5 mm	0.635 ± 0.047	0.281 ± 0.023
8–9 m	<0.5 mm	0.565 ± 0.009	0.250 ± 0.003
9–10 m	<2 mm	0.601 ± 0.006	0.314 ± 0.005
10–15 m	<0.5 mm	0.315 ± 0.004	0.123 ± 0.002
15–20 m	<0.5 mm	0.170 ± 0.005	0.064 ± 0.001

Appendix C: Particles >20 m from Detonation

Table C-1. Particles identified more than 20 m from the detonation site for 20FRA samples.

Detonation	Mass (g)	Number of Particles Identified
L01	26.318	159
L02	0	0
L03	0.361	2
L06	0	0
L07	9.276	68
L08	3.907	52

Appendix D: Particle-Size-Distribution Plots from Individual Detonations and Annuli

Figure D-1. PSDs from 81 mm Comp B low-order detonations. All samples are <2 mm unless otherwise noted.

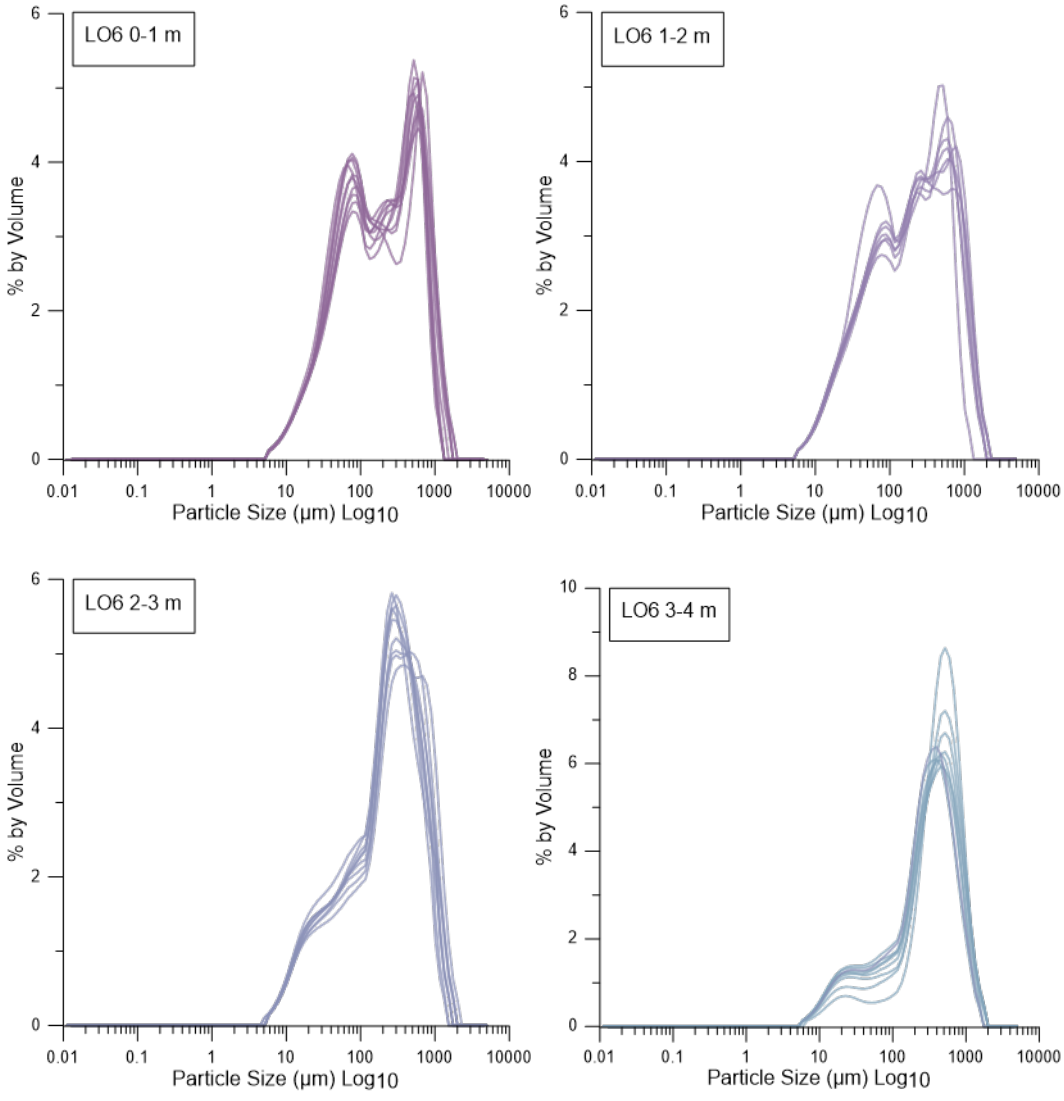

Figure D-1 (cont.). PSDs from 81 mm Comp B low-order detonations. All samples are <2 mm unless otherwise noted.

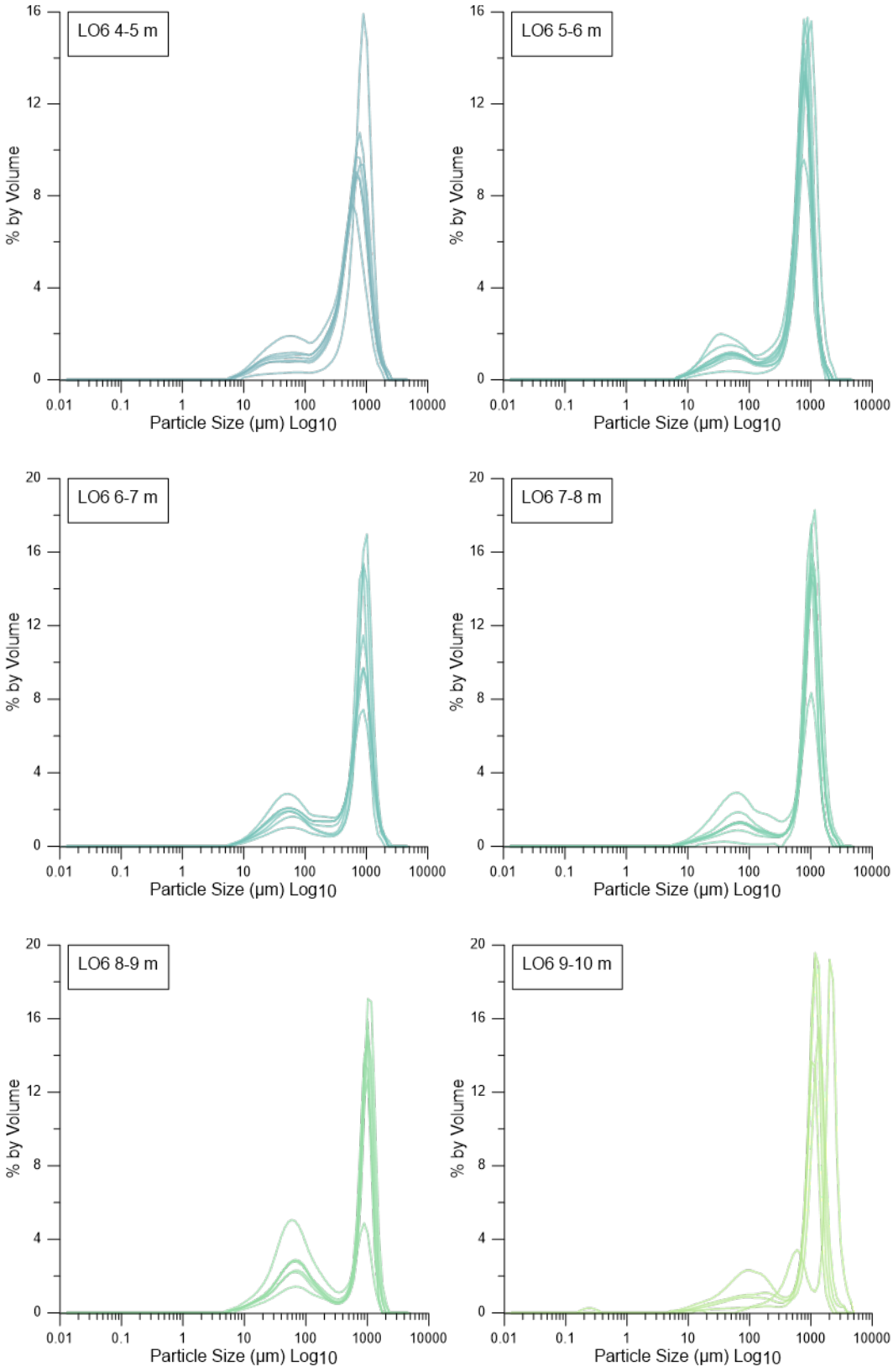

Figure D-1 (cont.). PSDs from 81 mm Comp B low-order detonations. All samples are <2 mm unless otherwise noted.

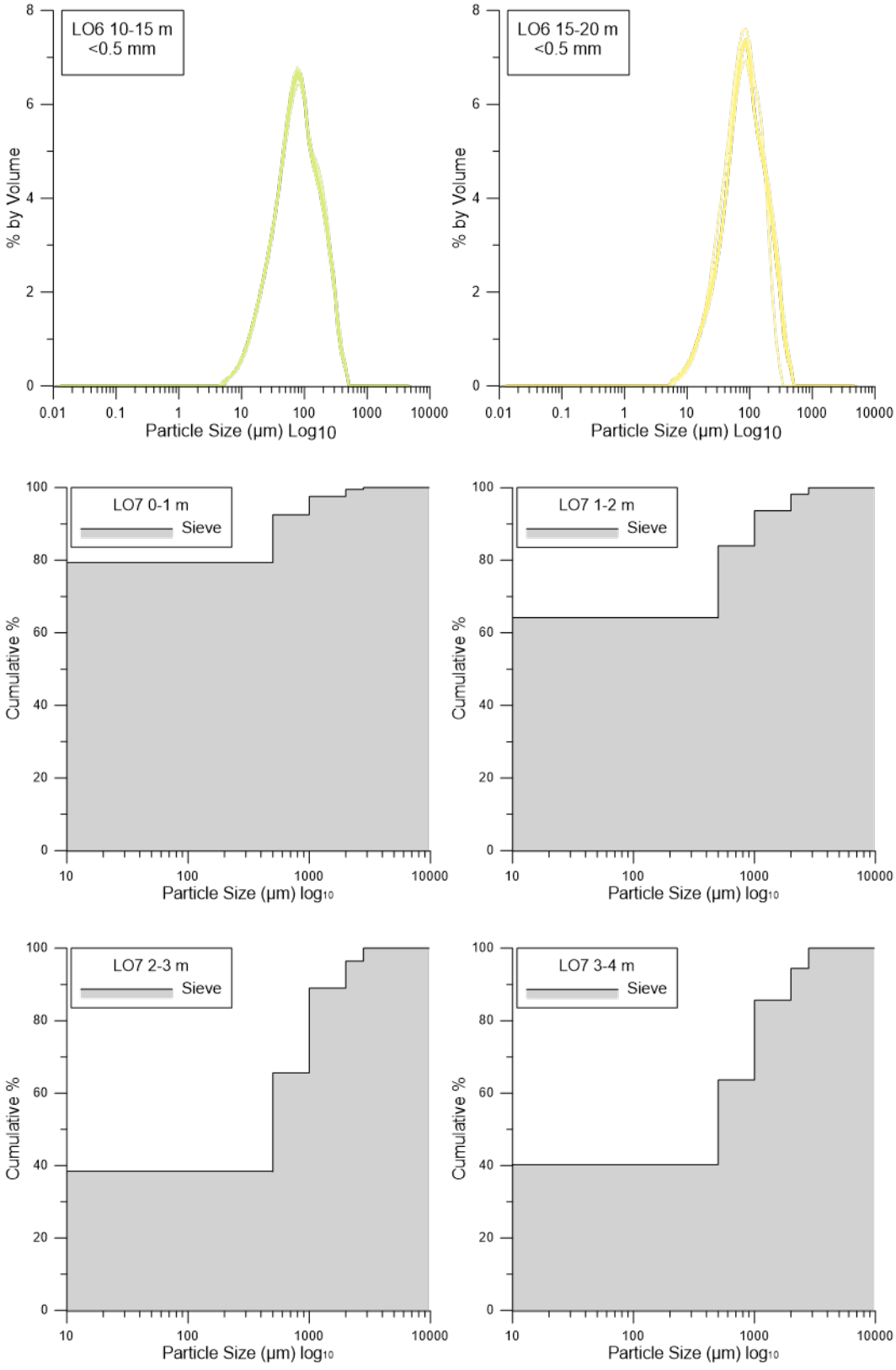

Figure D-1 (cont.). PSDs from 81 mm Comp B low-order detonations. All samples are <2 mm unless otherwise noted.

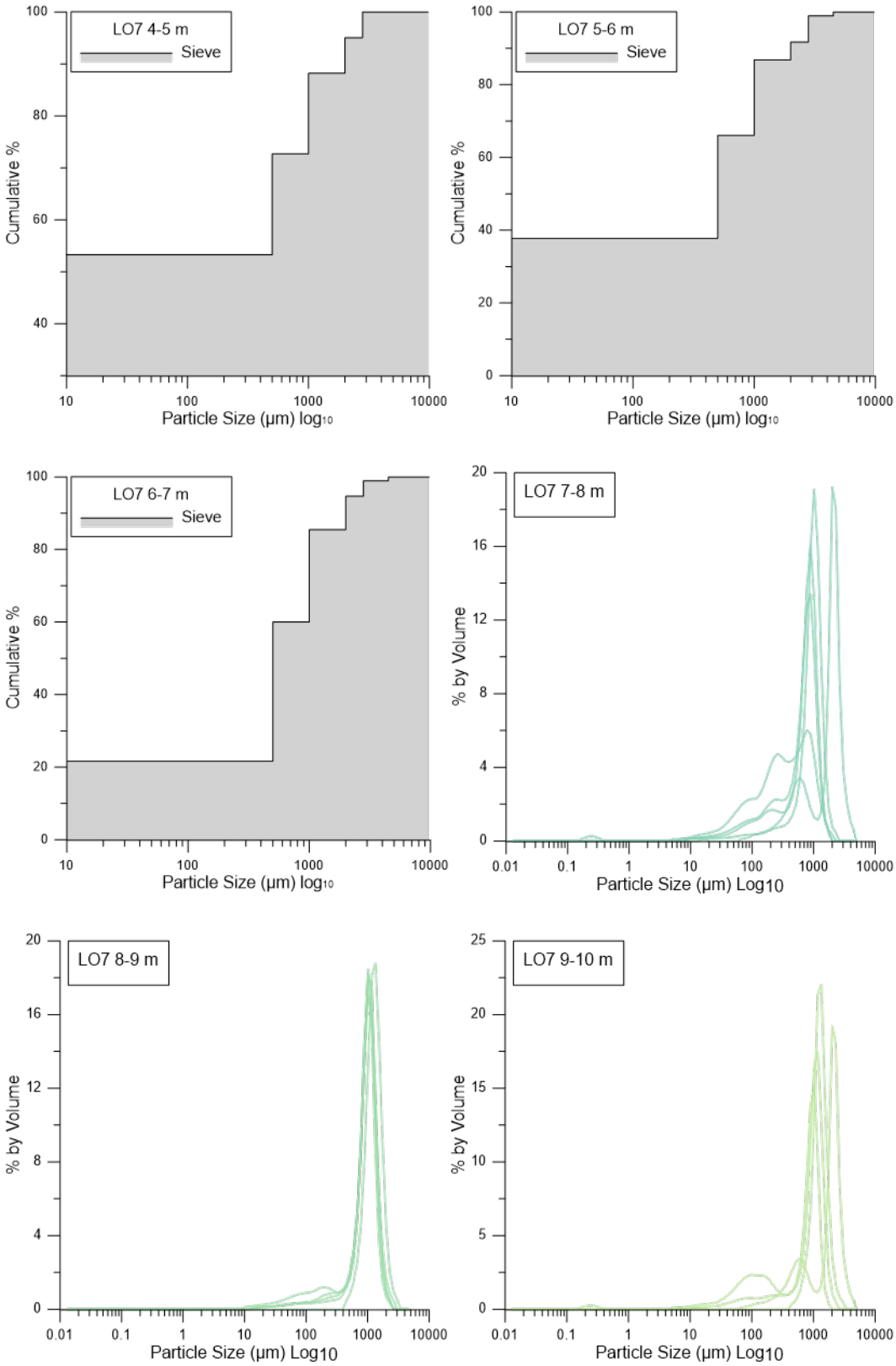

Figure D-1 (cont.). PSDs from 81 mm Comp B low-order detonations. All samples are <2 mm unless otherwise noted.

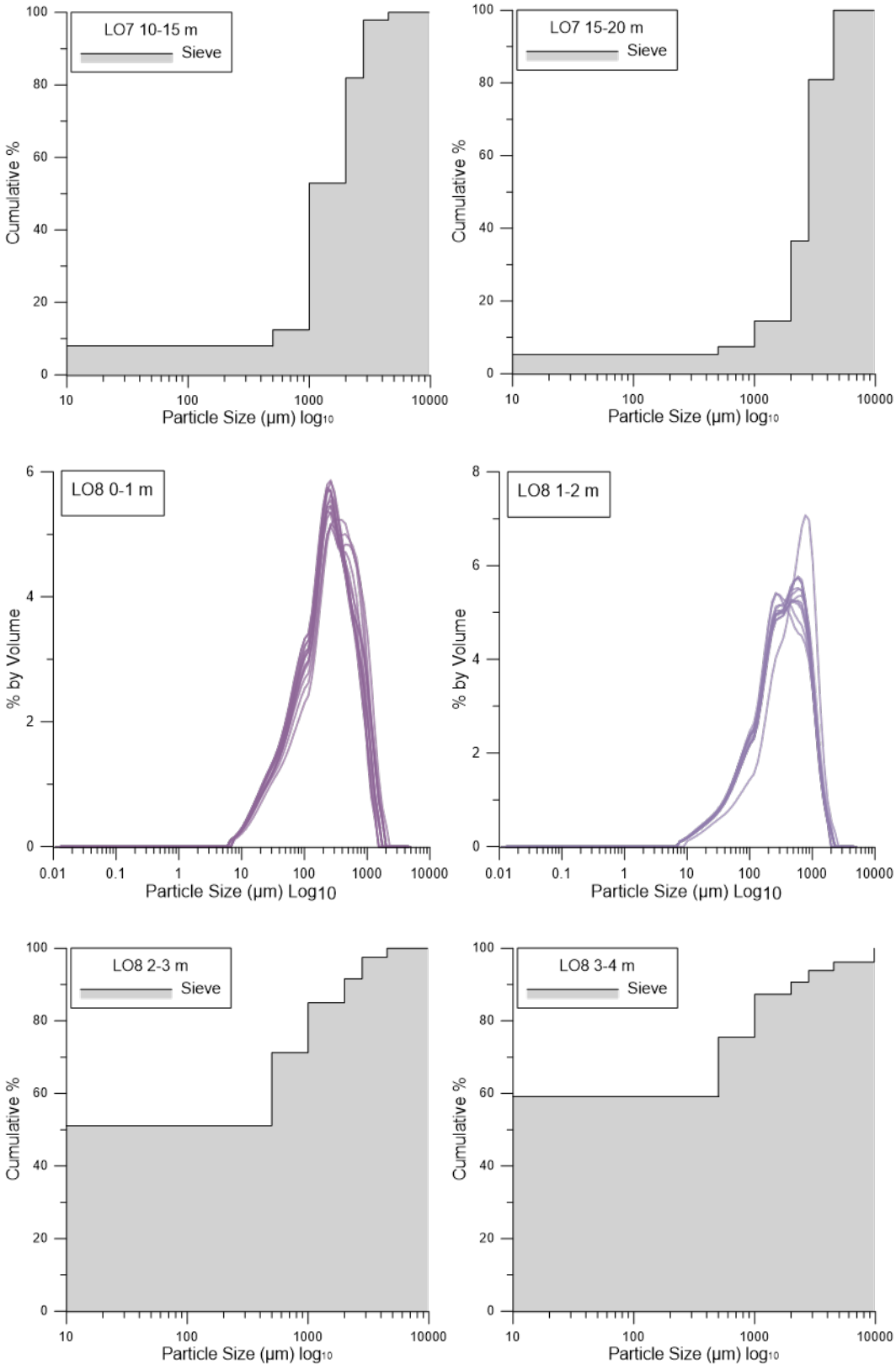

Figure D-1 (cont.). PSDs from 81 mm Comp B low-order detonations. All samples are <2 mm unless otherwise noted.

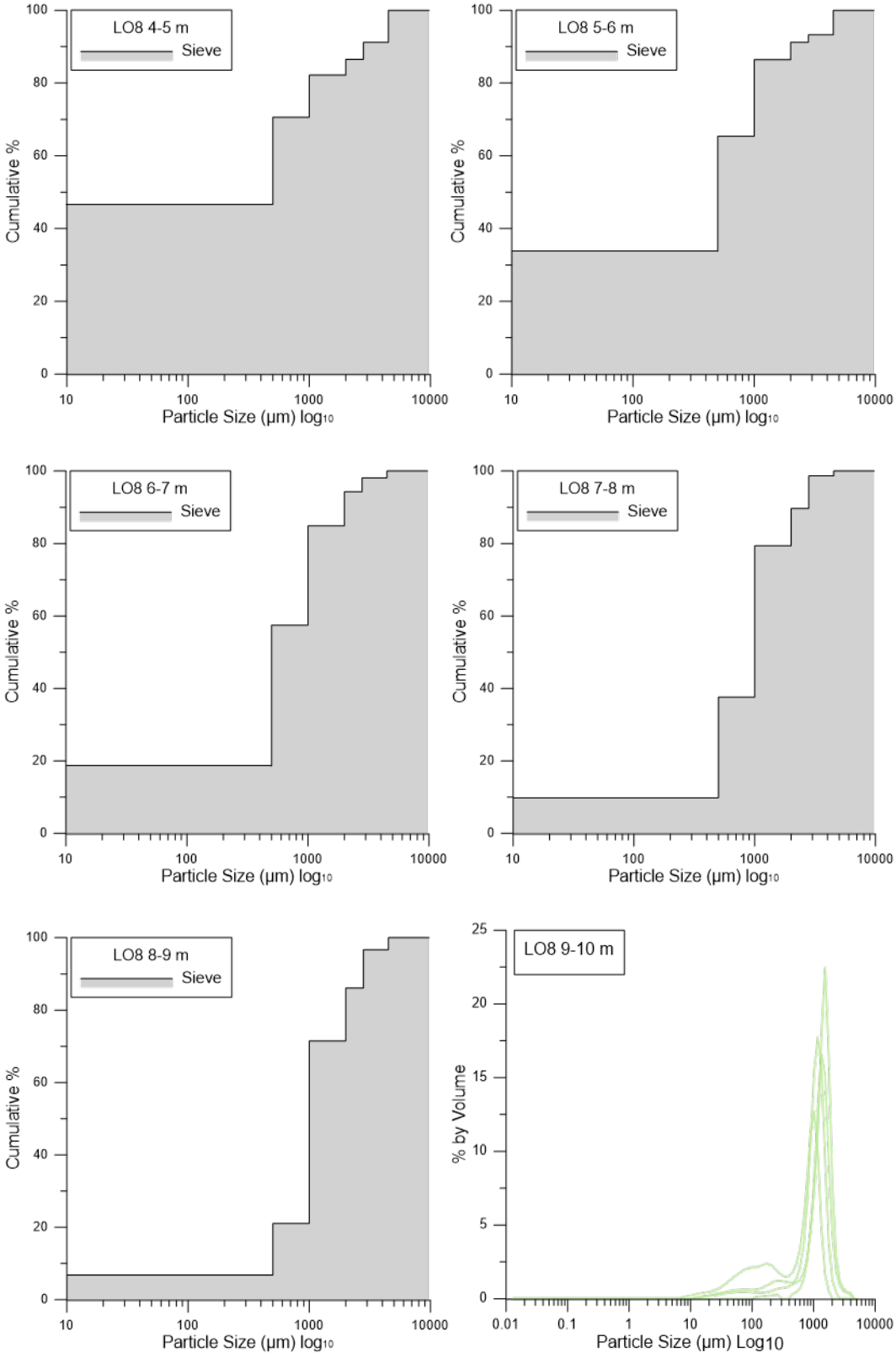

Figure D-1 (cont.). PSDs from 81 mm Comp B low-order detonations. All samples are <2 mm unless otherwise noted.

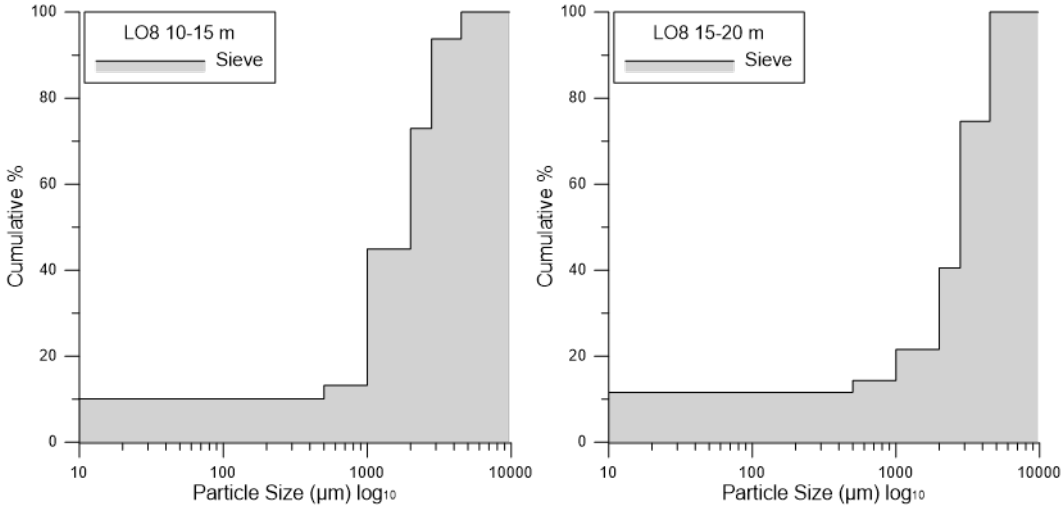

Abbreviations

Am	Amino
CFS	CRREL Fuze Simulator
CRREL	Cold Regions Research and Engineering Laboratory
D10	Diameter at which 10% of the distribution has smaller particle size
D50	Diameter at which 50% of the distribution has smaller particle size
D90	Diameter at which 90% of the distribution has smaller particle size
DNT	Dinitrotoluene
EDS	Energy Dispersive X-Ray Spectroscopy
EPA	Environmental Protection Agency
ERF	Eagle River Flats
ESTCP	Environmental Security Technology Certification Program
HMX	1,3,5,7-Tetranitro-1,3,5,7-Tetrazocane
HO	High Order
HPLC	High-Performance Liquid Chromatography
IMX-104	An insensitive munition formulation containing RDX, 3-Nitro-1,2,4-Triazol-5-One, and 2,4,-Dinitroanisole
JBER	Joint Base Elmendorf-Richardson
LCS	Laboratory Control Sample
LD-PSA	Laser-Diffraction Particle-Size Analysis
LO	Low Order
MS	Matrix Spike
MSD	Matrix Spike Duplicate
PSD	Particle-Size Distribution

RDX	1,3,5-Trinitro-1,3,5-Triazinane
RI	Refractive Index
SEM	Scanning Electron Microscope
SERDP	Strategic Environmental Research and Development Program
TNT	2,4,6-Trinitrotoluene
μCT	Microcomputed Tomography

REPORT DOCUMENTATION PAGE

Form Approved
OMB No. 0704-0188

1. REPORT DATE (DD-MM-YYYY)	2. REPORT TYPE	3. DATES COVERED (From - To)
August 2022	Technical Report / Final	FY18–FY21

4. TITLE AND SUBTITLE

Determination of Residual Low-Order Detonation Particle Characteristics from Composition B Mortar Rounds

5a. CONTRACT NUMBER

5b. GRANT NUMBER

5c. PROGRAM ELEMENT

6. AUTHOR(S)

Matthew F. Bigl, Samuel A. Beal, and Charles A. Ramsey

5d. PROJECT NUMBER

5e. TASK NUMBER

5f. WORK UNIT NUMBER

7. PERFORMING ORGANIZATION NAME(S) AND ADDRESS(ES)

US Army Engineer Research and Development Center (ERDC)
Cold Regions Research and Engineering Laboratory (CRREL)
72 Lyme Road
Hanover, NH 03755-1290

EnviroStat, Inc.
PO Box 339
Vail, AZ 85641

8. PERFORMING ORGANIZATION REPORT NUMBER

ERDC/CRREL TR-22-12

9. SPONSORING / MONITORING AGENCY NAME(S) AND ADDRESS(ES)

Strategic Environmental Research and Development Program
Environmental Security Technology Certification Program
Environmental Restoration Program Area
4800 Mark Center Drive, Suite 16F16
Alexandria, VA 22350-3605

10. SPONSOR/MONITOR'S ACRONYM(S)

SERDP-ESTCP

11. SPONSOR/MONITOR'S REPORT NUMBER(S)

12. DISTRIBUTION / AVAILABILITY STATEMENT

Approved for public release; distribution is unlimited.

13. SUPPLEMENTARY NOTES

Funding was provided by MIPRs W74RDV80715663, W74RDV80715688, W74RDV90156248, and W74RDV90497295.

14. ABSTRACT

Empirical measurements of the spatial distribution, particle-size distribution, mass, morphology, and energetic composition of particles from low-order (LO) detonations are critical to accurately characterizing environmental impacts on military training ranges. This study demonstrated a method of generating and characterizing LO-detonation particles, previously applied to insensitive munitions, to 81 mm mortar rounds containing the conventional explosive formulation Composition B. The three sampled rounds had estimated detonation efficiencies ranging from 64% to 82% as measured by sampled residual energetic material. For all sampled rounds, energetic deposition rates were highest closer to the point of detonation; however, the mass per radial meter varied. The majority of particles (>60%), by mass, were <2 mm in size. However, the spatial distribution of the <2 mm particles from the point of detonation varied between the three sampled rounds. In addition to the particle-size-distribution results, several method performance observations were made, including command-detonation configurations, sampling quality control, particle-shape influence on laser-diffraction particle-size analysis (LD-PSA), and energetic purity trends. Overall, this study demonstrated the successful characterization of Composition B LO-detonation particles from command detonation through combined analysis by LD-PSA and sieving.

15. SUBJECT TERMS

Command detonation; Composition B; Energetic material; Explosives, Military--Environmental aspects; Explosives, Military--Residues; Fate and transport; Laser diffraction; Low-order detonation; Particle-size analysis; Propellants--Residues; Range sustainment

16. SECURITY CLASSIFICATION OF:			17. LIMITATION OF ABSTRACT	18. NUMBER OF PAGES	19a. NAME OF RESPONSIBLE PERSON
a. REPORT	b. ABSTRACT	c. THIS PAGE			19b. TELEPHONE NUMBER (include area code)
Unclassified	Unclassified	Unclassified	SAR	58	